AD NUMBER
AD481648
LIMITATION CHANGES
TO: **Approved for public release; distribution is unlimited.**
FROM: **Distribution authorized to U.S. Gov't. agencies and their contractors; Administrative/Operational Use; APR 1966. Other requests shall be referred to Arnold Engineering Development Center, Arnold AFB, TN.**
AUTHORITY
AEDC per ltr dtd 4 Apr 1982

Muse

AEDC-TR-66-57

FULL-SCALE SIMULATED ALTITUDE INVESTIGATION OF THE CENTAUR-PAYLOAD SURFACE AND FUNCTIONAL DEGRADATION RESULTING FROM THE SATURN S-IVB RETRO ROCKET EXHAUST CONTAMINANTS

W. W. Muse
ARO, Inc.

May 1966

LARGE ROCKET FACILITY
ARNOLD ENGINEERING DEVELOPMENT CENTER
AIR FORCE SYSTEMS COMMAND
ARNOLD AIR FORCE STATION, TENNESSEE

NOTICES

When U. S. Government drawings specifications, or other data are used for any purpose other than a definitely related Government procurement operation, the Government thereby incurs no responsibility nor any obligation whatsoever, and the fact that the Government may have formulated, furnished, or in any way supplied the said drawings, specifications, or other data, is not to be regarded by implication or otherwise, or in any manner licensing the holder or any other person or corporation, or conveying any rights or permission to manufacture, use, or sell any patented invention that may in any way be related thereto.

Qualified users may obtain copies of this report from the Defense Documentation Center.

References to named commercial products in this report are not to be considered in any sense as an endorsement of the product by the United States Air Force or the Government.

FULL-SCALE SIMULATED ALTITUDE INVESTIGATION OF THE CENTAUR-PAYLOAD SURFACE AND FUNCTIONAL DEGRADATION RESULTING FROM THE SATURN S-IVB RETRO ROCKET EXHAUST CONTAMINANTS

W. W. Muse
ARO, Inc.

Pete

FOREWORD

The work reported herein was done at the request of the National Aeronautics and Space Administration (NASA), Marshall Space Flight Center (MSFC) under System 920E, Project 5991.

The results of tests presented were obtained by ARO, Inc. (a subsidiary of Sverdrup and Parcel, Inc.), contract operator of the Arnold Engineering Development Center (AEDC), AFSC, Arnold Air Force Station, Tennessee, under Contract AF 40(600)-1200. Engineering liaison was provided by NASA and The Boeing Company, under subcontract with NASA. Testing for this program was conducted from November 3 through 24, 1965, under ARO Project No. KA1548, and the manuscript was submitted for publication on February 21, 1966.

The author would like to acknowledge NASA/MSFC and The Boeing Company for their contributions in analyzing the surface degradation of the contamination and solar cell panels.

This technical report has been reviewed and is approved.

John W. Hitchcock
Major, USAF
AF Representative, RTF
DCS/Test

Jean A. Jack
Colonel, USAF
DCS/Test

ABSTRACT

A series of five tests was conducted in Propulsion Engine Test Cell (J-4) in support of a study to determine the surface contamination of the Centaur vehicle and its payload resulting from the deposition of retro exhaust particles during separation from the spent S-IVB stage. The test article consisted of a full-scale model, 120-deg segment of the S-IVB interstage adapter-Centaur-payload sections of the Saturn 1B-Centaur vehicle. An S-IVB retro motor was mounted in the adapter section at either a 0- or 11.5-deg angle upward from the model surface and was ignited at a pressure altitude of approximately 130,000 ft. The contamination of the model surface was primarily a gray deposit of iron and aluminum oxides. Predominant sizes of the particles deposited on the contamination panels were 1 to 10 μ. However, many particles ranged from 20 to 60 μ, and a few particles were as large as 400 μ. Particle erosion of the paint on the model surface was 12 to 14 μ in depth and occurred in a 4- to 30-ft interval downstream of the nozzle exit. The test results dependent upon retro motor firing angles of 0 and 11.5 deg, respectively, varied as follows: (1) maximum surface heating rate, 14.1 to 9.0 Btu/ft^2-sec; (2) maximum surface pressure, 0.29 to 0.14 psia; (3) degradation of solar cell panel performance, 26.6 to 6.0 percent; (4) laser beam attenuation, 22 to 12 percent; and (5) nominal change in surface reflectance of the model utilizing a laser beam, 27 to 19 percent.

CONTENTS

		Page
	ABSTRACT	iii
	NOMENCLATURE	vii
I.	INTRODUCTION	1
II.	APPARATUS	
	2.1 Test Article	2
	2.2 Installation	3
	2.3 Instrumentation	3
	2.4 Test Cell	5
III.	PROCEDURE	6
IV.	RESULTS AND DISCUSSION	
	4.1 Contamination Panel Degradation	7
	4.2 Solar Cell Performance	9
	4.3 Model Surface Pressure and Heat Rate Distributions	10
	4.4 Laser Experiments	11
	4.5 Exhaust Plume Radiance	13
	4.6 Exhaust Plume Characteristics	13
	4.7 Motor Performance	13
V.	SUMMARY OF RESULTS	14
	REFERENCES	15

ILLUSTRATIONS

Figure		
1.	Saturn 1B-Centaur Vehicle	17
2.	Centaur-Payload Shroud Arrangement	18
3.	Aerial View of Test Cell J-4	19
4.	Cutaway Drawing of Test Cell J-4	20
5.	S-IVB Interstage Adapter-Centaur-Payload Model	22
6.	Installation and Instrumentation Schematic	23
7.	Instrumentation Locations	25
8.	Identification of Contamination Panel Specimens	27
9.	Contamination Panel Configuration for the Charged Panel Experiment	29

Figure		Page
10.	Typical Solar Cell Panel	30
11.	Helium-Neon Gas Laser Units	31
12.	Post-Fire Contamination Inspection	33
13.	S-IVB Retro Motor Nozzle Exit Cone, Post-Fire	36
14.	Typical Microscopic Inspection of Contamination Panels	37
15.	Model Surface Paint Erosion	39
16.	Surface Reflectance of Various Contamination Specimens	40
17.	Solar Cell Panel Degradation	43
18.	Solar Cell Panel Calibration	44
19.	Typical Model Surface Pressure Distribution	46
20.	Typical Model Surface Heating Rate Distribution	47
21.	Typical Profile of Maximum Model Surface Pressures	48
22.	Typical Profile of Maximum Model Surface Heating Rates.	49
23.	Model Surface Pressure and Heating Rate Relationship	50
24.	Altitude Effect on Model Surface Heating Rates	51
25.	Test Equipment Setup for Laser Experiments.	52
26.	Contamination Panel III Reflectance of a Laser Beam	53
27.	Contamination Panel III Reflectance of Exhaust Plume Radiance	54
28.	Total Change in Model Surface Reflectance of a Laser Beam	55
29.	Laser Beam Transmittance through Exhaust Plumes	56
30.	Typical Exhaust Plume Characteristics for a 0-deg Angle Retro Motor Firing.	57
31.	Typical Exhaust Plume Characteristics for an 11.5-deg Angle Retro Motor Firing	59

Figure | Page

32. Motor Ambient Pressure Altitudes 61
33. Motor Chamber Pressure Envelope 62
34. Typical Spent Igniter 63

TABLES

I. Instrumentation Supplied by Various Agencies 65
II. Optical Recorders 66
III. Summary of Test Conditions and Results 67
IV. Test Summary of Contamination Panels 68
V. Model Surface Reflectance of a Laser Beam 69

NOMENCLATURE

Å	Angstrom, 10^{-8} cm
P	Pressure, psia
Q	Heat flux, Btu/ft^2-sec
T	Temperature, °F
t	Time, sec
μ	Microns, 10^{-6} M

SUBSCRIPTS

a	Ambient
f	Force
m	Mass
ms	Model surface
o	Zero
pm	Photomultiplier
r	Radiation
t	Total

SECTION I
INTRODUCTION

The Centaur vehicle is being considered as the third stage of the Saturn 1B launch vehicle. This addition would provide the National Aeronautics and Space Administration (NASA) with a payload capability for placing either a Pegasus- or Voyager-type spacecraft in a planetary orbit. One conception of the Saturn 1B-Centaur vehicle is to encase the Centaur and its payload in a two-piece, aerodynamic shroud (Figs. 1 and 2) which is the same diameter as the S-IVB stage. This shroud would be jettisoned during the second-stage operation to reduce the weight penalty. After explosive charges have structurally separated the S-IVB and Centaur stages, three retro motors, mounted on the forward interstage adapter, are proposed to decelerate the spent S-IVB stage and separate it from the Centaur and its payload. Since the Centaur and its payload would be exposed to the exhaust of the S-IVB retro motors during stage separation, concern has arisen as to the surface contamination and its effect on (1) heat transfer to the Centaur stage during its orbital coast period, and (2) degradation of the spacecraft solar cells performance.

A test program was initiated in the Propulsion Engine Test Cell (J-4) of the Large Rocket Facility (LRF) (Fig. 3, Ref. 1) in support of a study to determine the surface contamination of the Centaur and its payload caused by the deposition of retro motor exhaust particles during separation from the spent S-IVB stage. Five tests were conducted in the spray chamber of Test Cell J-4 (Fig. 4) at pressure altitudes of approximately 130,000 ft (Ref. 2).

The objectives of the test program were as follows:

1. Primary Objectives
   a. Evaluate the surface degradation (composition and relative particle size of the exhaust deposits and change in absorptivity/emissivity) of the specimens on the contamination panels.
   b. Determine the degradation of the solar cell panel performance.
   c. Determine model surface pressure and heating rate distributions resulting from retro motor exhaust impingement.
   d. Determine the effects of electrically charged panels on exhaust particle deposition.

e. Determine laser beam attenuation through the retro motor exhaust plume.

f. Determine change in surface reflectance of the model using a laser beam.

g. Determine the radiant heat transfer from the exhaust plume of the retro motor.

2. Secondary Objectives

a. Evaluate the degradation of ablative materials resulting from exhaust particle erosion and deposition.

b. Verify tailoff stability of the S-IVB retro motor at simulated altitude conditions.

c. Determine the optical characteristics of the retro motor exhaust plume.

SECTION II
APPARATUS

2.1 TEST ARTICLE

The test article (Fig. 5) was a full-scale model, 120-deg segment of the S-IVB interstage adapter-Centaur-payload sections of the Saturn 1B-Centaur vehicle with one S-IVB retro motor mounted in the interstage adapter section.

2.1.1 S-IVB Retro Motor

The S-IVB retro motor (TX-143-37), designed and developed by the Thiokol Chemical Corporation, contains a composite base solid propellant designated TP-L8006. Nominal chamber pressure of 1100 psia and thrust of 5000 lb_f are developed for approximately 2 sec. The nozzle has a throat area of 3.56 $in.^2$ and an area ratio of 5. The average propellant flow rate is 30 lb_m/sec.

2.1.2 S-IVB Interstage Adapter-Centaur-Payload Model

A full-scale model, 120-deg segment of the S-IVB interstage adapter-Centaur-payload sections of the Saturn 1B-Centaur vehicle (after shroud separation) was designed and fabricated by NASA for testing at AEDC. The model was fabricated (from 1/4-in. aluminum supported by an aluminum angle frame) in sections to facilitate

installation in the spray chamber of Test Cell J-4. Completely assembled, the model length was 53.5 ft, and the weight was approximately 3000 lb. The radius of the Centaur-payload segment of the model was 5 ft.

2.2 INSTALLATION

The S-IVB interstage adapter, Centaur, and payload sections of the model were lowered separately by the overhead crane down the exhaust diffuser to the deflector plate, assembled, and welded in place (Figs. 4 and 5). The retro motor support stand was mated with the S-IVB interstage adapter and aligned parallel with the centerline of the model. Mounting supports were installed and aligned for laser units, photomultiplier tube detectors, solar cell panel and excitation lamp bank, cameras, heat flux and pressure transducers, and contamination panels. After in-place checkouts of these instruments, a S-IVB retro motor was installed in the support stand (designed for vernier-type angular adjustments) at either 0- or 11.5-deg angles, depending on the particular test requirement.

2.3 INSTRUMENTATION

Instrumentation for this test program is described in the following sections. Instrumentation supplied by various agencies is summarized in Table I. The location of the instrumentation is presented in Figs. 6 and 7.

2.3.1 General

Test cell and motor chamber pressures and pressure distribution along the surface of the model were measured using strain-gage-type pressure transducers. These pressure transducers were calibrated at AEDC under laboratory conditions against a secondary standard prior to initial test cell installation.

Test cell and solar cell temperatures were sensed with Chromel®-Alumel® thermocouples.

In-place calibration of all recording systems just prior to each test consisted of substituting precision electrical resistance values to simulate known transducer load signals.

2.3.2 Contamination Panels

Electrically charged and passive contamination panels were used to determine the surface degradation (composition and relative particle sizes of the exhaust deposits and the change in absorptivity and emissivity) of the model. A schematic of the panel locations on the model surface is presented in Fig. 6. Passive contamination panels contained various painted, insulated, and ablative specimens (Fig. 8); the surface of the other contamination panels, as well as the model surface, was coated with white enamel paint (MIL-E-5556).

For the charged panel experiment, three panels were installed on the model surface (Figs. 6 and 9). Using a high voltage transformer, a positive, negative, and zero charge was placed on the three panels as indicated by utilizing a voltage divider and regulator.

2.3.3 Solar Cell Panels

The solar cell panels (Fig. 10) had 210 negative on positive (N on P) silicon-type solar cells arranged in five series of 42 cells with each series connected in parallel. The maximum solar cell panel output power is approximately 3300 mw at 15 v. The N on P silicon-type solar cells are sensitive to a radiation bandwidth of 400 to 1200 Å and convert approximately 10 percent of the total solar energy into power. To protect the solar cells against high energy, short wavelength radiation, a spectrally selected glass filter with a sharp transmittance cutoff below 400 Å and better than 95-percent transmittance at longer wavelengths is bonded to each cell. The glass filters are 60 mils thick and thereby provide considerable micrometeorite erosion protection for the solar cells.

The solar cell panels were calibrated relative to a standard panel both pre- and post-fire. The calibration consisted of determining the voltage-current (EI) characteristic curves for both the test panel and the standard panel at near identical conditions.

The solar cell panels used for this test program were spare Pegasus (meteoroid explorer probe) solar cell modules.

2.3.4 Laser Equipment

Two gas laser units provided high intensity, collimated light sources for the model surface reflectance and laser beam attenuation measurements. The changes in surface reflectance and laser beam attenuation

were measured by photomultiplier tubes (Q_{pm}-1 and -3, respectively) with narrow band-pass filters (10 Å) centered at 6328 Å. For the laser beam attenuation measurement, a Perkin-Elmer helium-neon (He-Ne) continuous wave (cw) gas laser unit (Fig. 11a) with an 0.5-mw output at 6328 Å was used. The unit used for the surface reflectance measurements was a Spectra-Physics He-Ne cw gas laser (Fig. 11b) with a 3-mw output at 6328 Å.

2.3.5 Calorimeters

Asymptotic-type calorimeters were used to measure the heating rate distribution along the surface of the model. Calibration curves from the manufacturer were used for data reduction.

2.3.6 Radiation Measurements

Exhaust plume radiance reflected from the model surface was measured with a photomultiplier tube (Q_{pm}-2) with a narrow band-pass filter (200 Å) centered at 8400 Å. The photomultiplier tube was calibrated in-place with a standard blackbody source.

Total radiance of the exhaust plume was measured by a Gardon gage-type radiometer. Calibration curves from the manufacturer were used for data reduction.

2.3.7 Optical Recorders

Optical recorder devices were used to record characteristics of the exhaust plume. Recorder type, designation, frame rate, and film type are summarized in Table II. Timing marks (100 cycles per second) were provided on the photographic film to determine the exact framing rate of the optical recorder.

2.4 TEST CELL

Test Cell J-4 (Fig. 4a) is the largest altitude test cell operating in the free world. It is a vertical test cell primarily designed for testing large rocket engines and entire propulsion systems (present thrust capability of 500,000 lb_f with a growth potential of 1.5 million lb_f) at pressure altitudes in excess of 100,000 feet. An additional testing capability has been demonstrated in the 2,000,000-cu-ft spray chamber of the test cell for investigating exhaust plume phenomena and spacecraft contamination. The spray chamber is normally used for water-spray cooling the exhaust gases from large rocket engines. However,

for tests in the spray chamber, the water cooling systems are secured to provide a dry environment. By using the calibration ejectors (low mass flow steam ejectors in the exhaust duct system) in series with the exhaust machinery, pressure altitudes of approximately 130,000 feet may be obtained for an indefinite period of time.

SECTION III
PROCEDURE

As the test hardware arrived at the AEDC, it was visually inspected and stored to await buildup in preparation for testing. All S-IVB retro motors were subjected to a stringent radiographic inspection with the 25-Mev Betatron machine. The S-IVB interstage adapter-Centaur-payload model was assembled on the deflector plate in the spray chamber, and all instrumentation was installed, connected, and checked out (Section 2.2).

After motor buildup, it was transported to the test cell and installed in the support stand. The motor instrumentation was connected, and final verification checkouts of instrumentation and control systems were performed.

Upon completion of atmospheric calibrations, the test cell was evacuated by the exhaust machinery to approximately 0.4 psia prior to operation of the Test Cell J-4 calibration ejectors. After obtaining a minimum cell pressure (approximately 0.04 psia) with the calibration ejectors, altitude calibrations were accomplished and the final countdown sequence was performed.

Immediately after the motor firing, the air inbleed valve was partially opened (allowing air circulation down through the exhaust diffuser and up through the spray chamber) to remove the retro motor exhaust from the spray chamber and to essentially eliminate contamination fallout on the surface of the model. After the test cell was returned to atmospheric conditions, the test hardware was visually inspected and documented photographically. The spent S-IVB retro motor was removed from the test cell and returned to the rocket proparation area for post-fire inspection. The contamination panels were returned to NASA and The Boeing Company for evaluation of the composition and relative particle size of the exhaust deposits and change in surface absorptivity and emissivity. The solar cell panel was calibrated to determine the degradation of the panel performance. The model surface was cleaned and a new set of contamination panels was installed on the model for the subsequent tests.

SECTION IV
RESULTS AND DISCUSSION

Five tests were conducted in the spray chamber of Test Cell J-4 with retro motor ignitions at pressure altitudes of approximately 130,000 ft. Data collected to accomplish the test objectives are discussed in the following sections. A summary of the test conditions and results is presented in Table III.

4.1 CONTAMINATION PANEL DEGRADATION

Passive contamination panels were used to measure the model surface degradation resulting from the deposition of exhaust particles during the retro motor firings. These panels contained various painted, insulated, and ablative specimens (Fig. 8). The types of panels used for each test are summarized in Table IV.

4.1.1 General

Post-fire inspection of the contamination panels and the model surface revealed exhaust particle streaks, gray and black exhaust particle deposits, specimen ablation and discoloration, and paint blisters (Fig. 12). Gray exhaust particle deposits identified primarily as aluminum and iron oxides (Section 4.1.2) were the most predominant type of contamination observed along the model surface. This type deposit was distributed over the entire model with the exception of the region near the base of the interstage adapter. In this region, black exhaust particle deposits were concentrated. These deposits were attributed to recirculation deposition of low momentum particles from the igniter and throat liner during the ignition and tailoff phases of motor operation, respectively. Microscopic inspection of these stratified deposits of exhaust particles revealed that igniter particles (magnesium and boron) were deposited initially. In addition, the buildup of black deposits in this region was observed by optical recorders during motor tailoff.

The exhaust particle streaks observed on the surface of the model after tests -01 and -02 were attributed to the charred paint on the exterior of the nozzle exit cone (Fig. 13) being entrained into the retro exhaust and deposited on the model surface. The removal of the paint from the nozzle exit cone for subsequent tests eliminated the streaking phenomena.

Specimen discoloration was a common occurrence on tests in which the specimen-type panels were used. Discoloration resulted from a combination of surface heating and contamination.

Paint blisters occurred on the S-13 paint specimen which was mounted at a 45-deg angle to the retro exhaust flow and approximately 50 ft downstream from the nozzle exit plane.

4.1.2 Exhaust Particle Deposits

Emission spectographic, X-ray defraction, and chemical spot-testing techniques were used to determine the constituents of the exhaust particle deposits. The major constituents were aluminum and iron oxides with traces of iron and aluminum chloride and silicates, carbon, magnesium, boron, and titanium oxide.

Microscopic investigation of the particle size (Fig. 14) indicated that the majority of the particles were 1 to 10 μ in size. However, many particles ranged in size from 20 to 60 μ, and a few particles were as large as 400 μ.

4.1.3 Panel Surface Erosion

Microscopic inspection of the disc-type contamination panels (Fig. 14) revealed erosion of the painted surface by the retro exhaust particles. Maximum erosion of 12 to 14 μ in depth occurred on panel IV. The erosion was observed on panels II through VII. The painted surface of the model eroded to the zinc chromate primer and bare aluminum in a 5- to 15-ft interval downstream of the nozzle exit plane (Fig. 15) during the course of the test program.

4.1.4 Absorptivity and Emissivity

Analysis of the change in surface absorptivity of various specimens on the contamination panels has not been completed and, therefore, cannot be included in this report. However, preliminary data were obtained by using a portable reflectometer to analyze the change in surface reflectance of one specimen per contamination panel. Pre- and post-fire reflectance data as a function wavelength for the bare aluminum, S-13 paint, white enamel, zinc chromate, and insulflor specimens are presented in Fig. 16. A reference panel, coated with white enamel paint (MIL-E-5556), was positioned outside the exhaust plume on the deflector plate to measure the contamination fallout on the model after the retro motor firings. The change in surface reflectance of the reference panel and the Johnson curve (Ref. 3) of solar radiation are also included in Fig. 16 for comparison purposes.

Analysis of the change in surface emissivity for the various specimens on the contamination panels has not been completed. However, preliminary data indicated no appreciable change in the emissivity of the specimens with the exception of bare aluminum which increased from 0.12 to approximately 0.17.

4.1.5 Charged Panel Effect

Because of the limited amount of data obtained, the results of the experiment were inconclusive.

4.2 SOLAR CELL PERFORMANCE

Three identical solar cell panels, used separately in tests -01, -02, and -03, were located on the model surface (approximately 36 ft downstream from the nozzle exit plane) in a position comparable with two much larger solar cell panels of the Pegasus satellite on the Saturn 1B-Centaur vehicle. The Pegasus satellite has four large solar cell panels with 6300 cells on each panel as compared to 210 solar cells on each test panel. The orientation of the solar cell panel relative to the flow of the S-IVB retro motor exhaust was unique for each of these three tests. For tests -01 and -02, the panels were installed parallel to the model surface, and the retro motors were fired at 11.5- and 0-deg angles, respectively, upward from the model surface. For test -03, the panel was installed perpendicular to both the model surface and the retro motor exhaust flow.

Post-fire inspection of the solar cell panels for tests -01 and -02 revealed nonuniform, gray, exhaust particle deposits (primarily aluminum and iron oxides) on the panels and no physical damage to the solar cells. For these tests, degradation of the solar cell panels performance was 6.0 and 26.6 percent, respectively. For test -03, post-fire inspection revealed considerable damage to the solar cells in addition to uniform, gray, exhaust particle deposits. Degradation of the solar cell panel performance for this test was 89.7 percent. Although the concentration of the exhaust particle deposits on the solar cell panels increased in the order of the firings, the severe 89.7-percent degradation of the solar cell panel performance resulted mainly from the extensive damage to the solar cells. A comparison between the solar cell panel degraded on test -03 and the standard calibration panel is presented in Fig. 17.

A calibration rack, consisting of a 3500-w lamp bank with a water filter to sufficiently reduce the infrared or heat radiation incidence

upon the solar cells, was used to calibrate the solar cell panels (Fig. 18a). Degradation of the solar cell panel performance relative to the standard panel was determined using the change in maximum output power measured during pre- and post-fire calibrations of both panels. Typical EI characteristic curves performed on the solar cell panels during these calibrations are presented in Fig. 18b.

A 2000-w lamp bank was suspended approximately 20 ft directly above the solar cell panel to excite the solar cells prior to, during, and after the retro motor firings. However, the intensity of the lamp bank was inadequate to excite the panels to a sufficient output power level required to obtain qualitative resolution for solar cell panel performance measurements. The luminosity of the exhaust plume was approximately an order of magnitude greater than the lamp bank in the 400- to 1200-Å bandwidth.

4.3 MODEL SURFACE PRESSURE AND HEAT RATE DISTRIBUTION

Pressure and heat flux transducers defined the model surface pressure and heating rate distributions resulting from the exhaust impingement of the S-IVB retro motor. Of particular interest were the distinct data trends (Figs. 19 and 20) of the measured pressures and heating rates which occurred for retro motor firings at 0- and 11.5-deg angles. Profiles of maximum measured pressure and heating rate at each sensor locale on the model surface, i.e., in a 4.0- to 11.5-ft interval downstream of the nozzle exit plane, are presented in Figs. 21 and 22. The location of the Mach disc, as observed from optical recorders (Section 4.6), several feet beyond the last pressure and heat flux sensors indicates that extrapolation of these curves would not completely define the pressure and heating rate profiles along the model surface. Although the effect of the Mach disc on surface heating was not defined, its very nature (increase in temperature and pressure) and observed intensity are indicative of its significance.

Measured heating rates along the model surface were essentially a direct function of the local pressure (Fig. 23). The local pressures were combinations of model surface static and dynamic pressures. The dynamic pressure component resulted from the impingement angle of the retro motor exhaust and therefore decreased with an increase in distance from the nozzle exit plane.

A study of the test data was conducted to determine the effect that pressure altitude had on the measured exhaust impingement heating rates on the model surface. A noticeable pressure altitude effect was observed for the tests with retro motor firings at an 11.5-deg angle.

The results of the study are presented in Fig. 24. Extrapolation of these curves indicates the heating rates to be expected at higher altitudes.

For the tests with retro motor firings at a 0-deg angle, it was observed that the heating rates increased with a decrease in pressure altitude (Fig. 20). This increase is attributed to a reduction in the free expansion characteristics of an exhaust plume and resulted in the movement of the exhaust impingement plane toward the pressure and heat flux transducers and an increase in the exhaust plume static pressure.

4.4 LASER EXPERIMENTS

The laser experiments were conducted during this test program to determine (1) change in surface reflectance of the model, and (2) laser beam attenuation through a retro motor exhaust. Two gas laser units provided high intensity, collimated light sources for these experiments.

4.4.1 Surface Reflectance

Disc-type contamination panels, designated I through VIII, were mounted on the model to implement the surface reflectance experiment. The objectives of the experiment were to determine (1) the change in surface reflectance of panel III as a function of motor firing time and (2) the total change in surface reflectance of each panel along the model surface.

To determine the reflectance of panel III as a function of motor firing time, measurements were taken during the firings with both the laser beam incident on the panel and the detector (Q_{pm}-1) viewing the panel at 45-deg angles (Fig. 25). Inconclusive data were obtained on tests -01 and -02 as a result of interference experienced by the intense luminosity of the exhaust plume. For subsequent tests, interference was reduced sufficiently by the addition of a limited view adapter and 10-Å band-pass filter to the detector. The surface reflectance of the panel was measured during test -03. To determine the plume radiance effects, the panel reflectance was measured on a subsequent test with the same retro motor firing configuration but without the laser unit on. The difference between these measurements (Fig. 26) was considered to be the surface reflectance of a laser beam as a function of time. The initial change in reflectance was attributed to the deposition of igniter particles on the panel as indicated by the

microscopic inspection of the stratified exhaust particle deposits. During motor operation, the deposition of exhaust particles on the panel eroded the igniter deposits (thereby increasing the reflectance temporarily) as well as paint from the panel (Fig. 14).

The model surface reflectance of the exhaust plume radiance was measured by another detector (Q_{pm}-2) viewing panel III at a 45-deg angle (Fig. 25). Reflected exhaust plume radiance data are presented in Fig. 27. The peaks which occurred at retro motor ignition and tailoff were attributed to the intense luminosity of the Mach disc observed from optical recorders. These peaks correlated in time with the location of the Mach disc in the field of view of the detector.

The total change in surface reflectance of the remaining panels was determined by interchanging their positions, one at a time, with panel III and recording surface reflectance of the laser beam pre- and post-fire. The data from these measurements are presented in Fig. 28 and Table V. As indicated by these curves, the heaviest concentration of deposits was located at the base of the interstage adapter for the tests with retro motor firings at a 0-deg angle, and approximately 5 ft downstream from the adapter for tests with retro motor firings at an 11.5-deg angle (Section 4.1.1).

4.4.2 Laser Attenuation

The arrangement of laser unit No. 2 and the detector (Q_{pm}-3) for measuring the laser beam attenuation through the retro motor exhaust plume is presented in Fig. 25. The laser beam transversed the exhaust plume at approximately 8 ft downstream from the nozzle exit plane.

Inconclusive data were obtained on tests -01, -02, and -03 as a result of interference experienced by the intense luminosity of the exhaust plume. For subsequent tests, the plume radiation was separated from the laser beam by the addition of a limited view adapter and a 10-Å band-pass filter to the detector and a 50-cps chopper on the laser unit.

Post-fire inspection of the laser unit revealed a film of exhaust particles on the clear sections of the Plexiglas® disc used to chop the laser beam. Spectrographic and density count analysis indicated a predominance of particles in the 1- to 2-μ size range which numbered 88 particles/cm^2. Recorded data revealed approximately 50-percent attenuation of the laser beam reflectance after the motor firings. The data were corrected on the assumption that the particles were deposited on the Plexiglas disc linearly with time. The corrected data

of laser transmittance through the exhaust plume are presented in Fig. 29. The laser beam attenuation for tests with 0- and 11.5-deg angle firings was 22 and 12 percent, respectively.

4.5 EXHAUST PLUME RADIANCE

Inconclusive data were obtained from total radiance of the exhaust plume measurement as a result of the inaccuracy of the radiometer in the range of the measured radiation. During each test, the radiometer operated in the lower 0.25 percent of its full-scale range.

4.6 EXHAUST PLUME CHARACTERISTICS

Optical data defined the exhaust core formed by the more luminous aluminum oxide particles, aerodynamic recompression of the gases on the plume centerline (Mach disc), and a smoke ring phenomena which occurred during motor ignition. Photographs showing the typical exhaust plume characteristics for retro motor firings at both 0- and 11.5-deg angles are presented in Fig. 30.

4.7 MOTOR PERFORMANCE

The motors were successfully ignited at pressure altitudes of approximately 130,000 ft. The ambient pressure altitudes experienced by the motor during each firing are presented in Fig. 31.

Motor chamber pressure data indicated that the motors performed satisfactorily. The envelope of motor chamber pressure measured during this test program is presented in Fig. 32. The observed smooth chamber pressure tailoff indicates shutdown stability of the S-IVB retro motor at altitude conditions.

Post-fire inspection of the motors revealed that a portion of the igniters had remained intact and that unburned propellant slivers remained in the motor case. A post-fire photograph of a typical igniter is presented in Fig. 33.

SECTION V
SUMMARY OF RESULTS

The results of the five tests at simulated altitude conditions in the spray chamber of Test Cell J-4 are summarized as follows:

1. The data obtained from this program demonstrated the capability for investigating surface contamination and exhaust plume impingement heating effects on full-scale space vehicles at simulated altitude conditions in the spray chamber of the Test Cell J-4.
2. Removal of the paint from the exterior of the nozzle exit cone eliminated the exhaust particle streaking phenomena on the model surface.
3. The major constituents of the exhaust particle deposits on the contamination panels were iron and aluminum oxides.
4. The predominant size of the exhaust particles deposited on the contamination panels was approximately 1 to 10 μ. However, many particles ranged in size from 20 to 60 μ, and a few particles were as large as 400 μ.
5. Erosion of contamination panels was as deep as 12 to 14 μ and occurred over a 4- to 30-ft interval downstream from the nozzle exit plane.
6. The performance degradation of the solar cell panels installed on the model parallel to the surface was 26.6 and 6.0 percent for the tests with retro motor firings at 0- and 11.5-deg angles, respectively.
7. Surface pressure and heating rate distribution on the model was markedly different for tests with retro motor firings at 0- and 11.5-deg angles. Profiles of maximum surface pressures and heating rates along the model surface were defined in a 4.0- to 11.5-ft interval downstream from the nozzle exit plane.
8. The laser beam attenuation through the exhaust plume was 22 and 12 percent for the tests with retro motor firing at 0- and 11.5-deg angles, respectively.

9. An unsuccessful attempt was made to determine the effect of an electrostatic charge on contamination of surfaces

10. A communication laser beam was indicated to be practical for interim communication during a "blackout" in the staging phase of space flight

REFERENCES

1. Test Facilities Handbook (5th Edition). "Rocket Test Facility, Vol. 2." Arnold Engineering Development Center, July 1963.

2. Dubin, M., Sissenwine, N., and Wexler, H. "U. S. Standard Atmosphere, 1962." December 1962.

3. Johnson, F. S. "The Solar Constant." Journal of Meteorology, Vol. II, No. 6, December 1954, pp. 431-439.

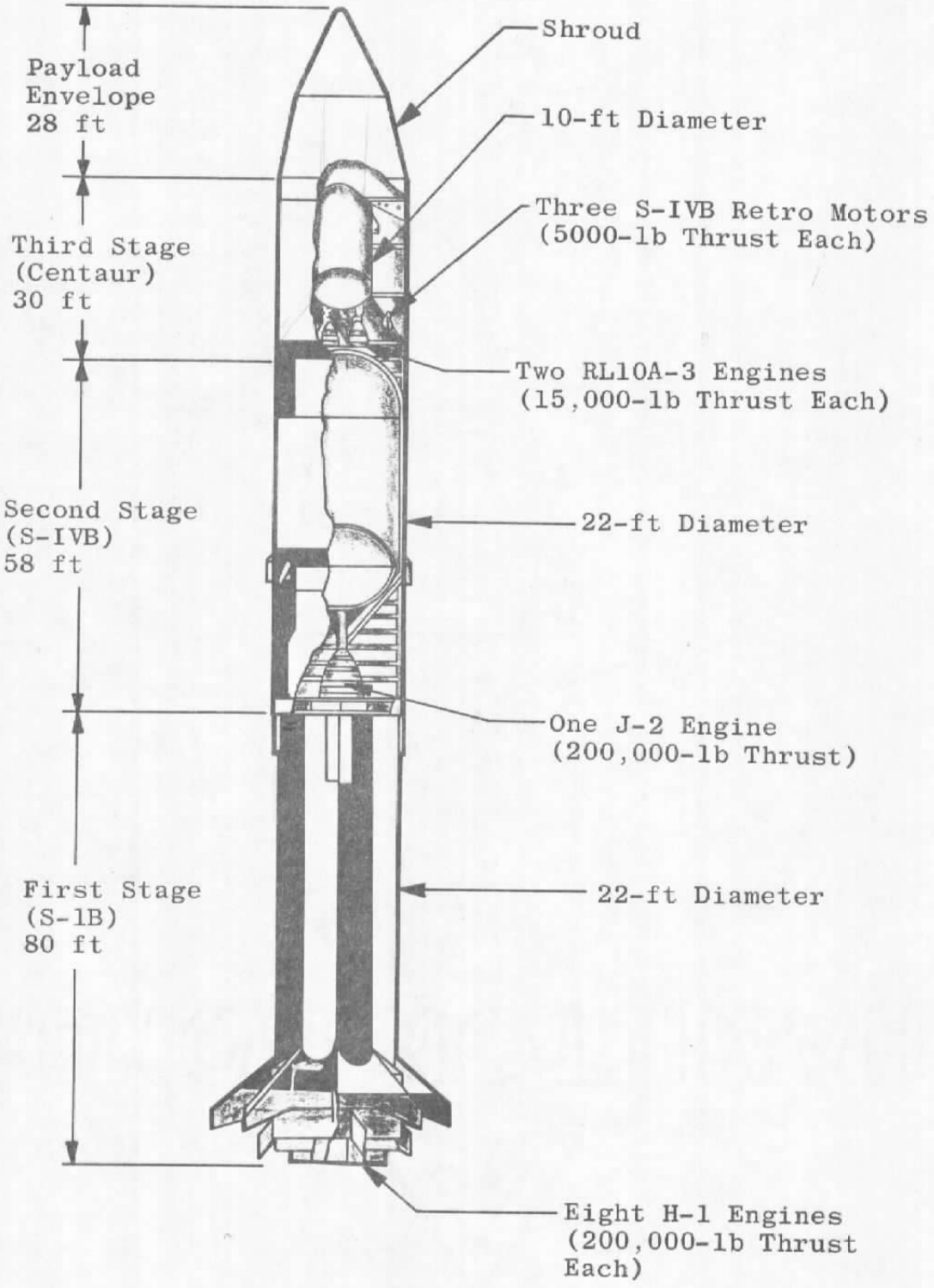

Fig. 1 Saturn 1B-Centaur Vehicle

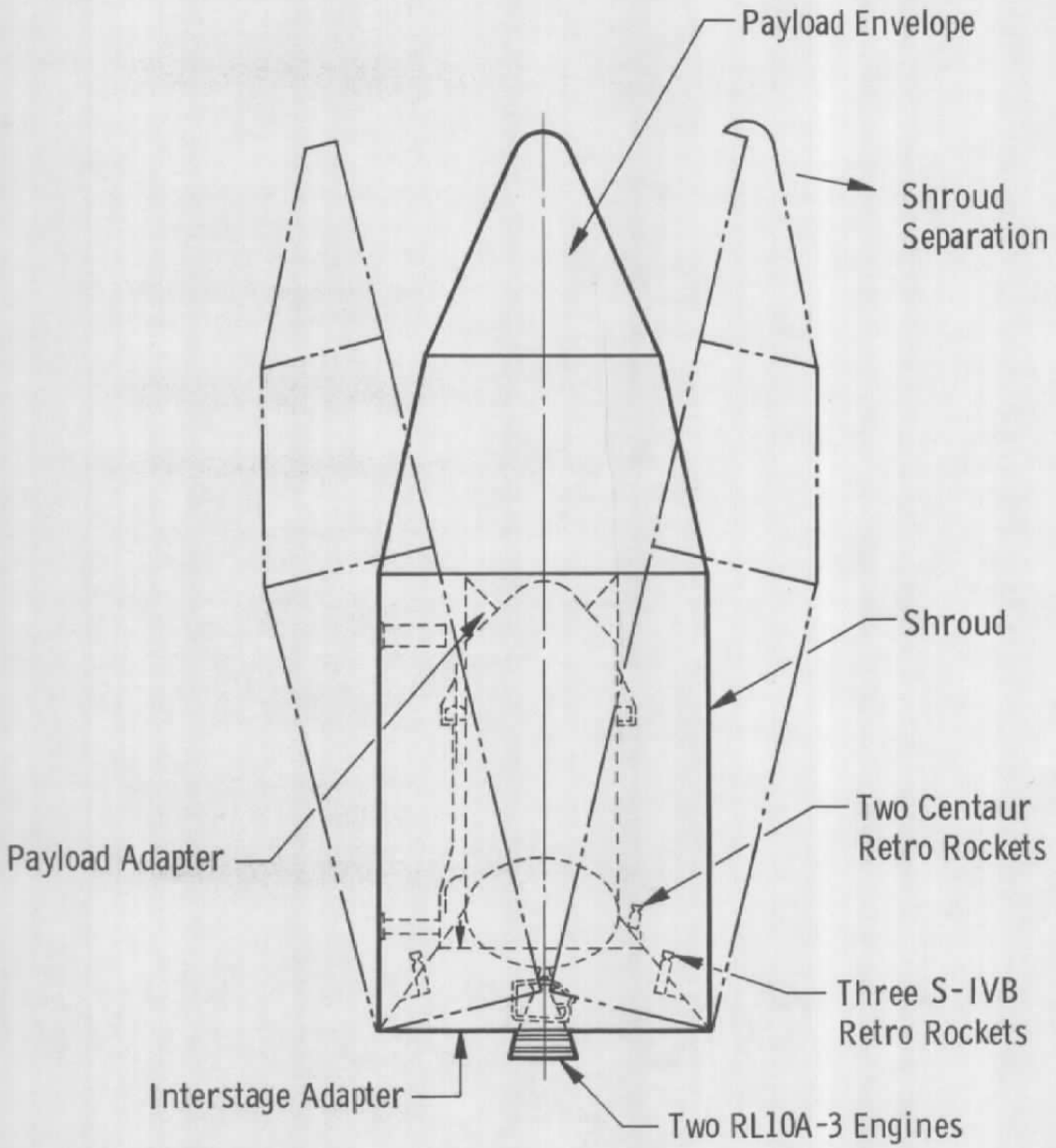

Fig. 2 Centaur-Payload Shroud Arrangement

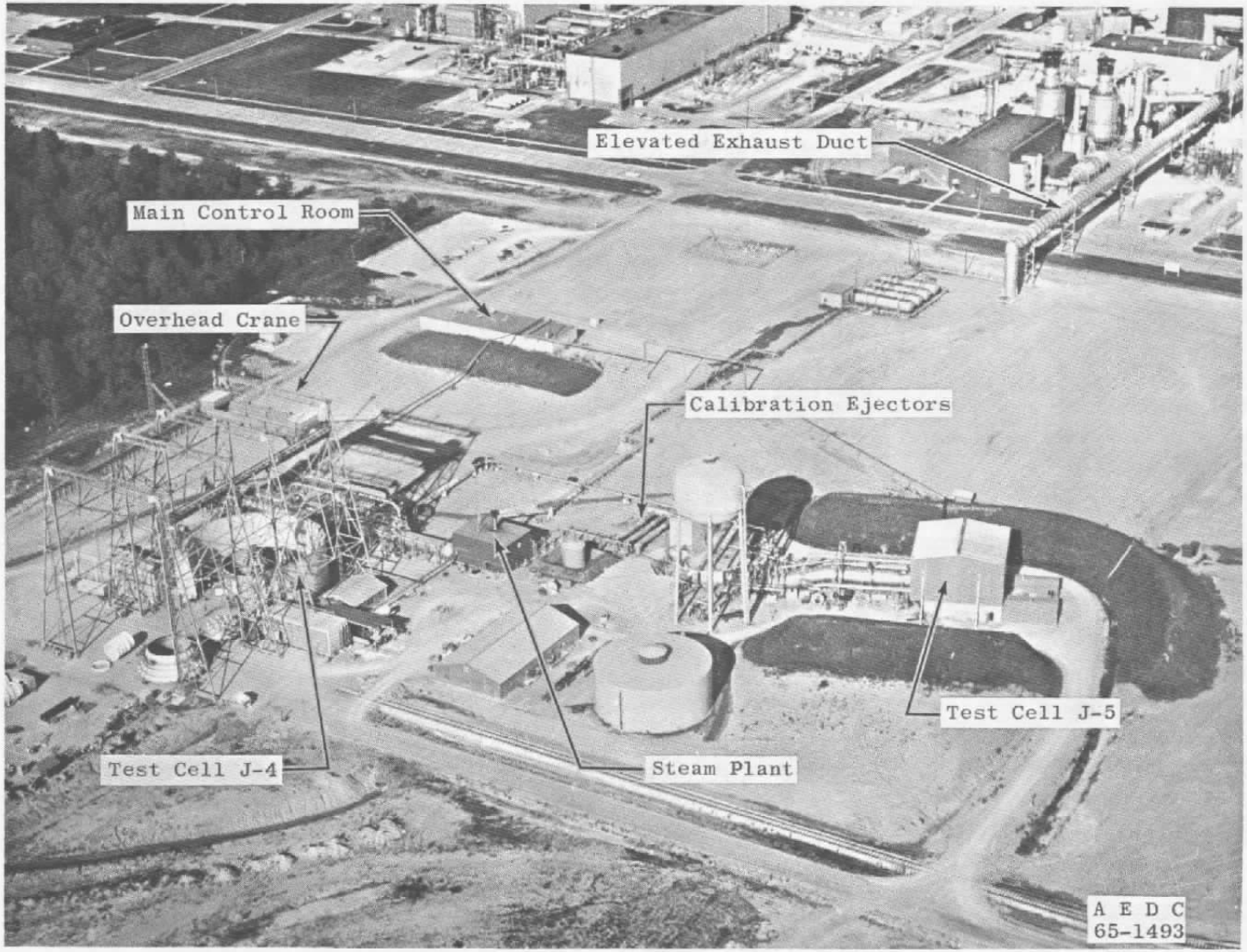

Fig. 3 Aerial View of Test Cell J-4

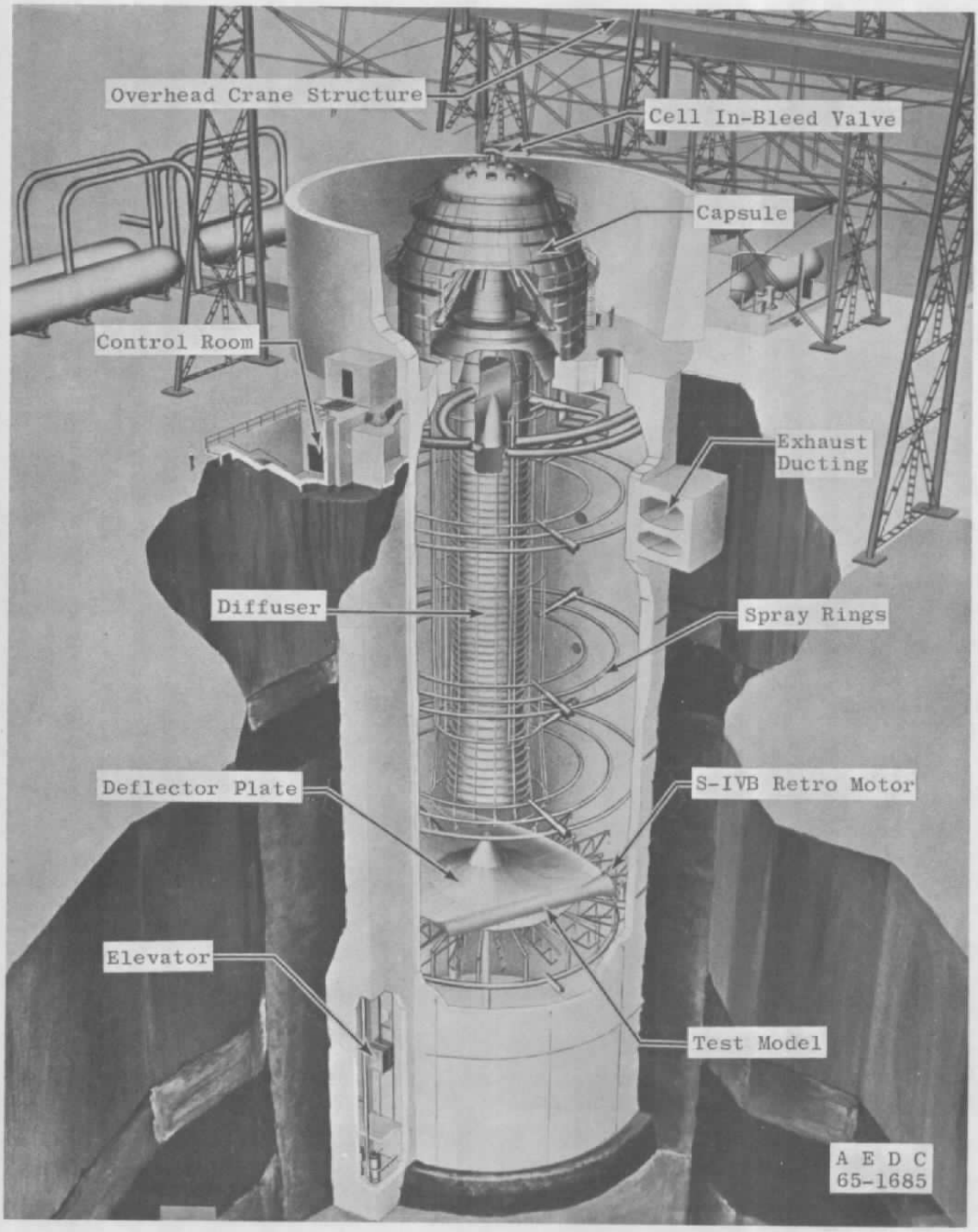

a. Test Cell Complex

Fig. 4 Cutaway Drawing of Test Cell J-4

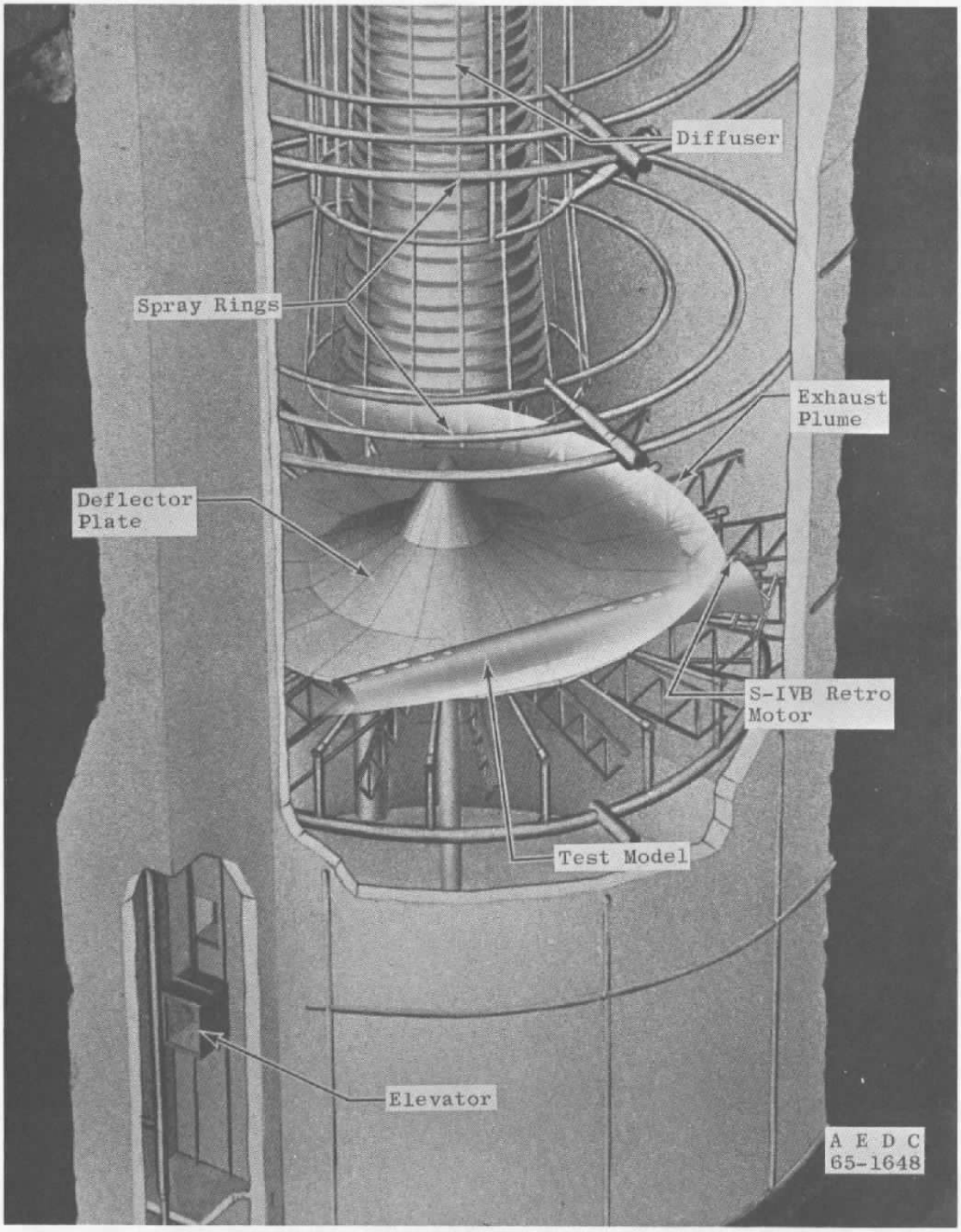

b. Deflector Plate Test Site

Fig. 4 Concluded

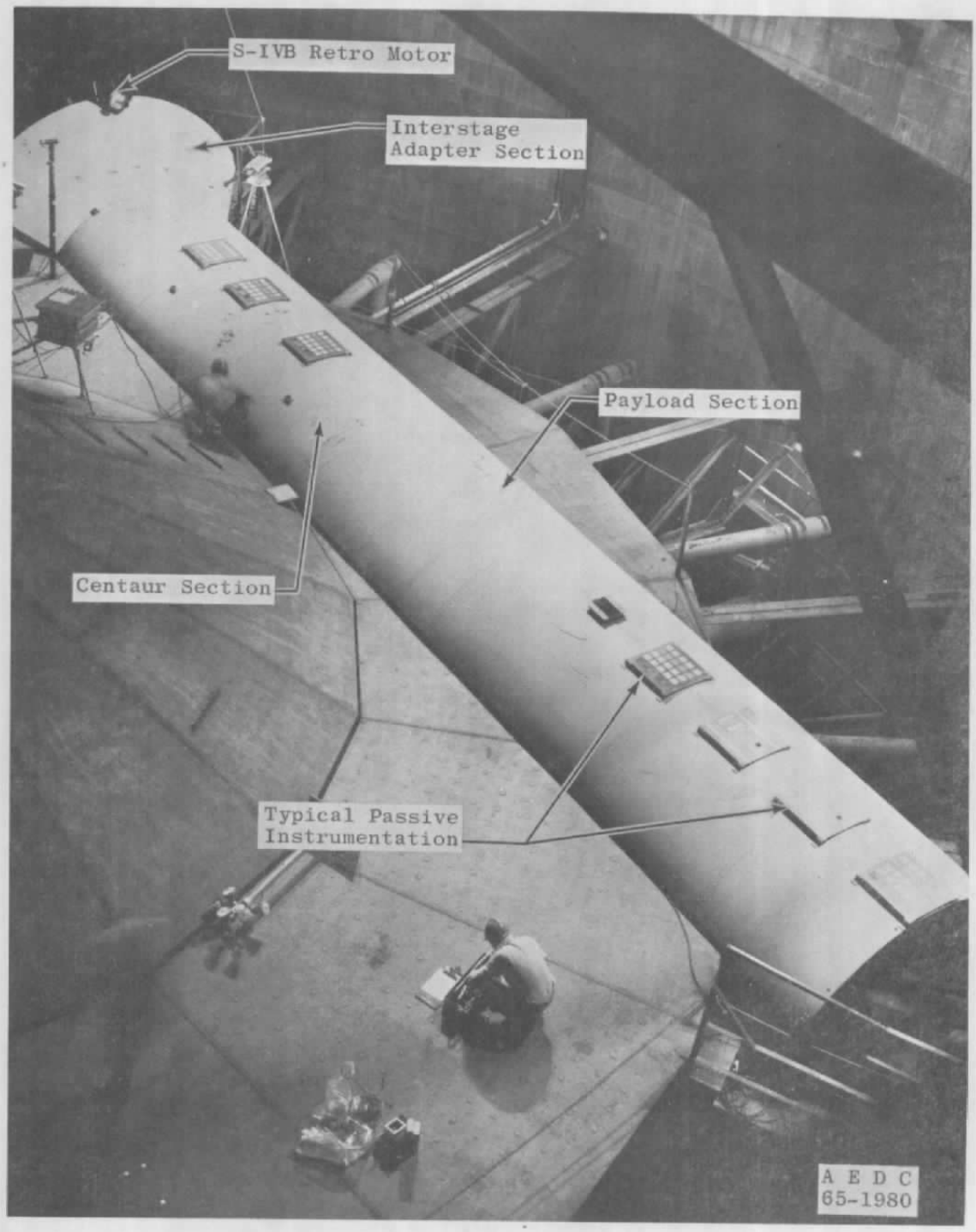

Fig. 5 S-IVB Interstage Adapter-Centaur-Payload Model

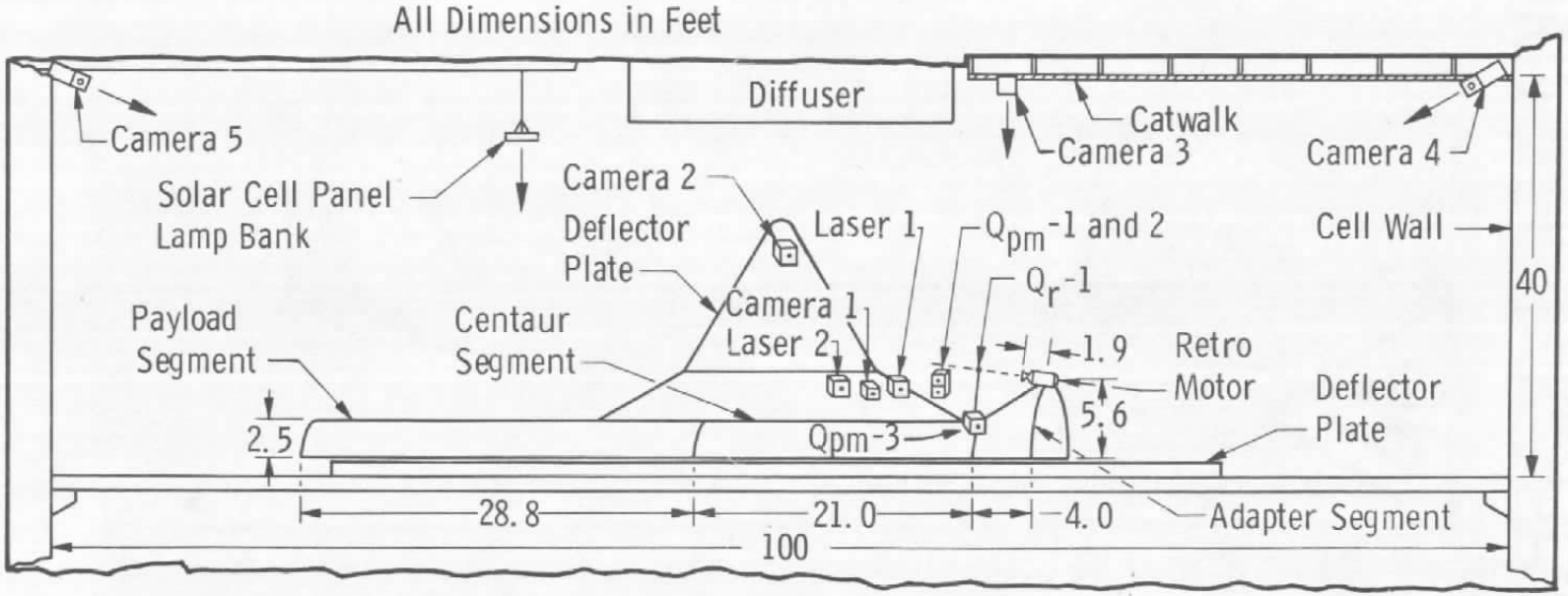

a. Elevation View

Fig. 6 Installation and Instrumentation Schematic

Active Instrumentation	Q_r-1	Q_t-1	Q_t-2	Q_t-3	Q_t-4	Q_t-5	P_{ms}-1	P_{ms}-2	P_{ms}-3	P_{ms}-4	P_{ms}-5	P_{ms}-6	P_{ms}-7	Q_{pm}-1	Q_{pm}-2	Q_{pm}-3
Location, ft (D. S. from N. E.)	3.7	4.4	4.9	5.4	7.2	10.3	4.4	4.9	5.4	6.5	7.2	10.3	11.3	8.1	8.1	~8.1
Contamination Panels	I	II	III	IV	V	VI	VII	VIII	A	B	C	D	E	X	Y	C. P.*
Location, ft (D. S. from N. E.)	2.2	4.6	8.1	10.6	15.0	21.2	29.2	34.4	8.8	12.7	17.7	40.3	50.8	44.0	47.4	23.5

*Charged Panels

All Dimensions in Feet

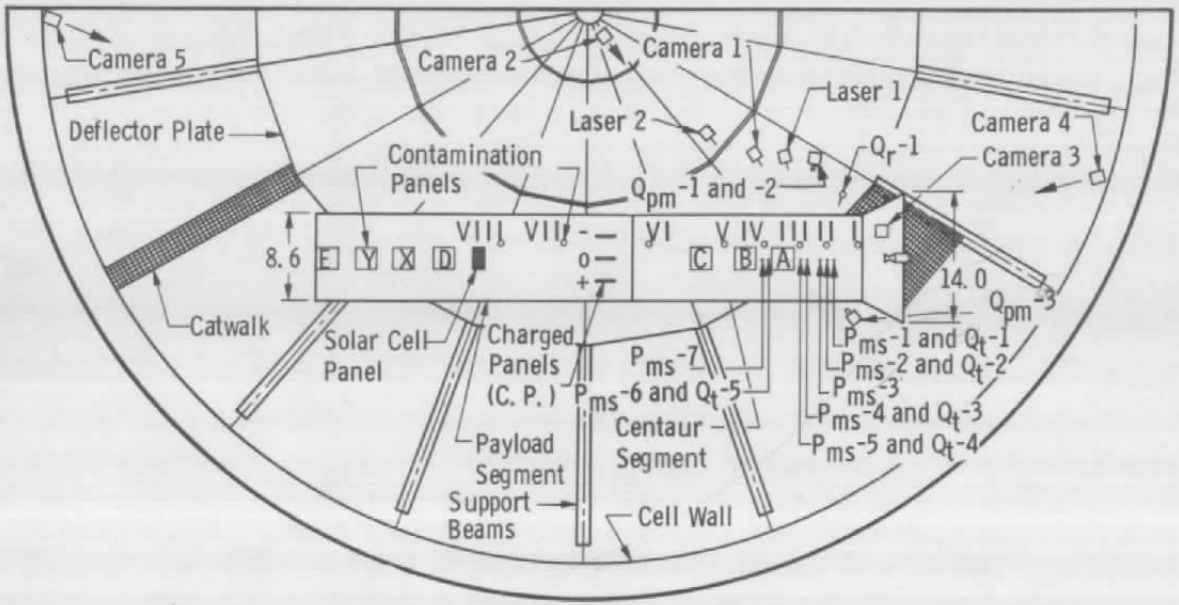

b. Plan View

Fig. 6 Concluded

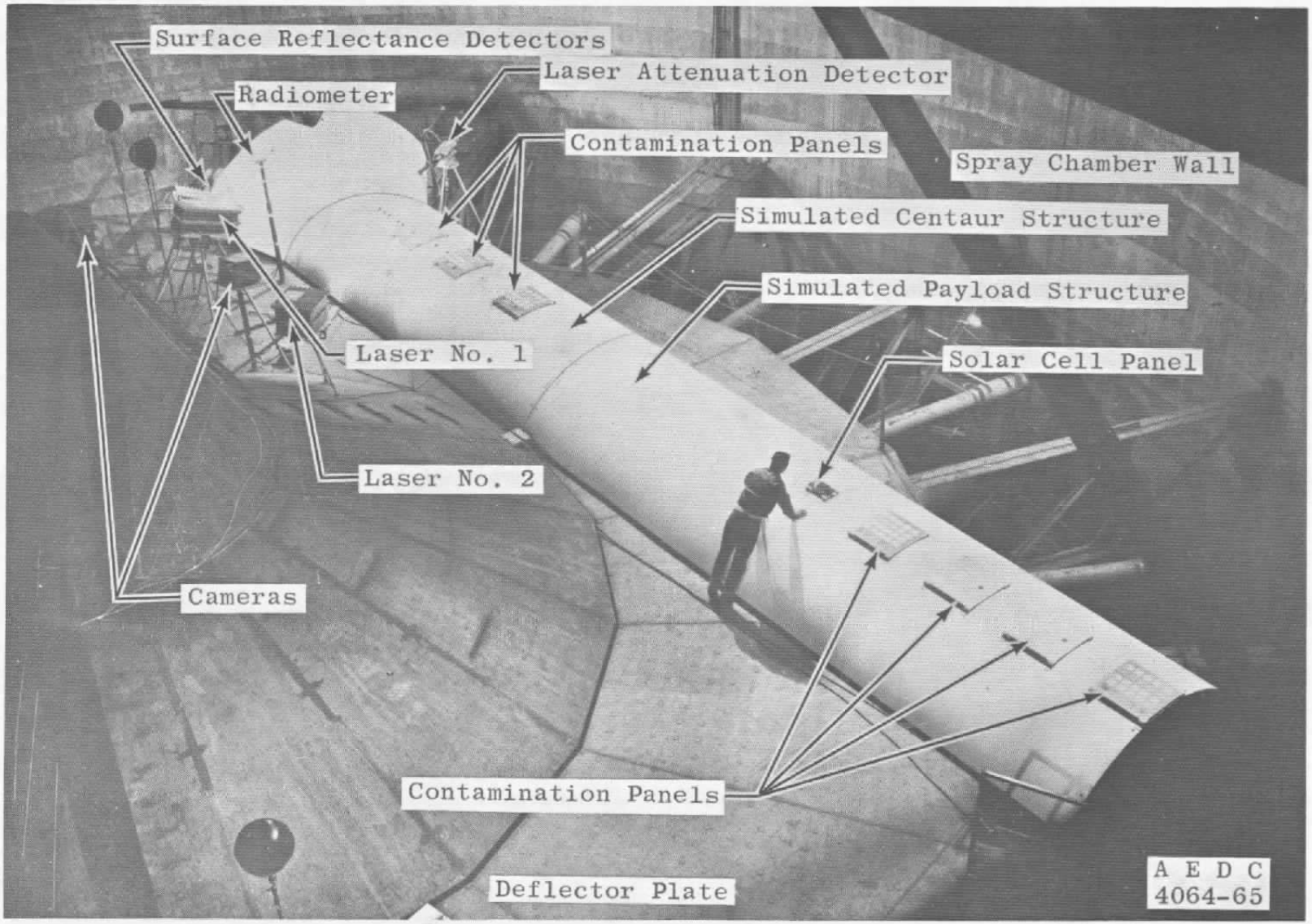

a. Contamination Panels, Laser Units, and Cameras

Fig. 7 Instrumentation Locations

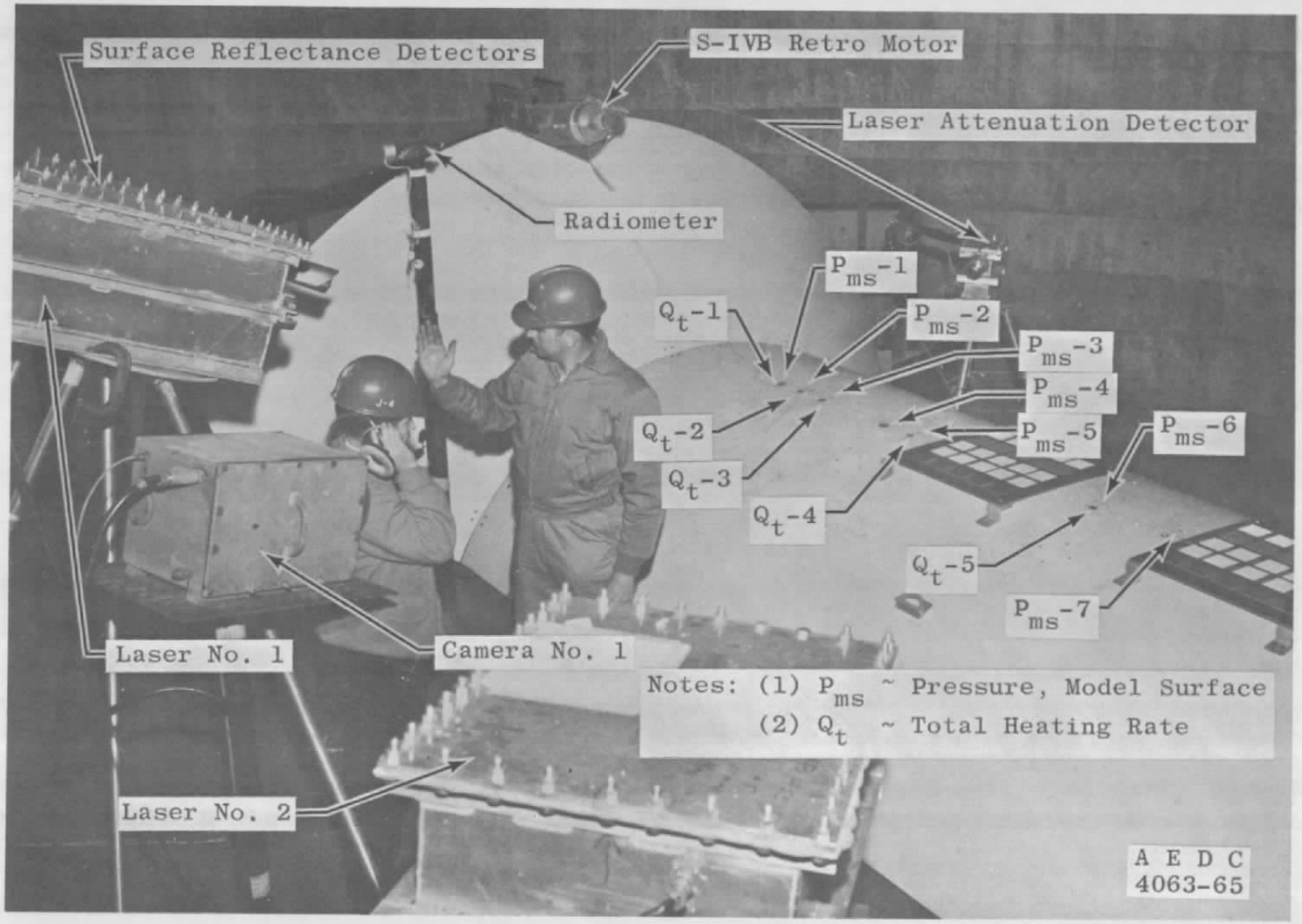

b. Model Surface Pressure and Heat Flux Sensors

Fig. 7 Concluded

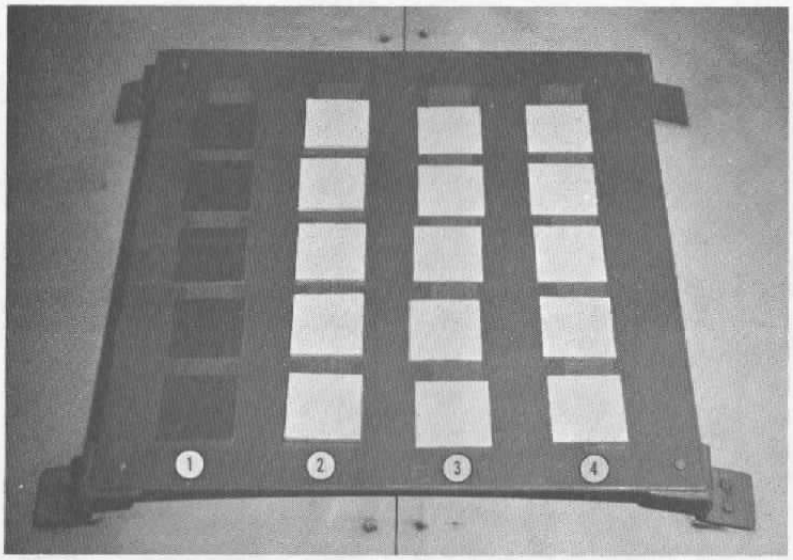

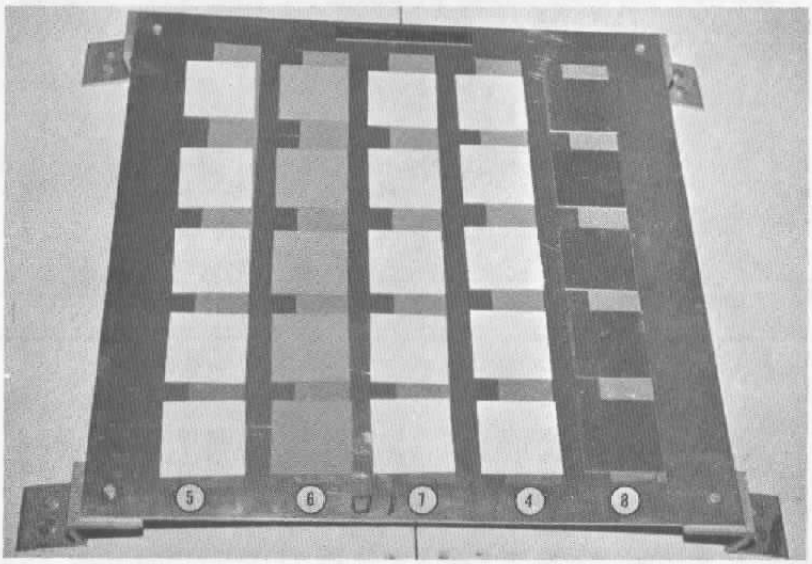

Column Number	Specimen Identification
1	Aluminum Paint
2	M-31 Insulation
3	Porcelain Enamel
4	S-13 Paint
5	Insulfor Coating
6	$ZnCrO_4$ Primer
7	White Enamel Paint
8	Bare Aluminum

a. Painted and Insulated Specimens

Fig. 8 Identification of Contamination Panel Specimens

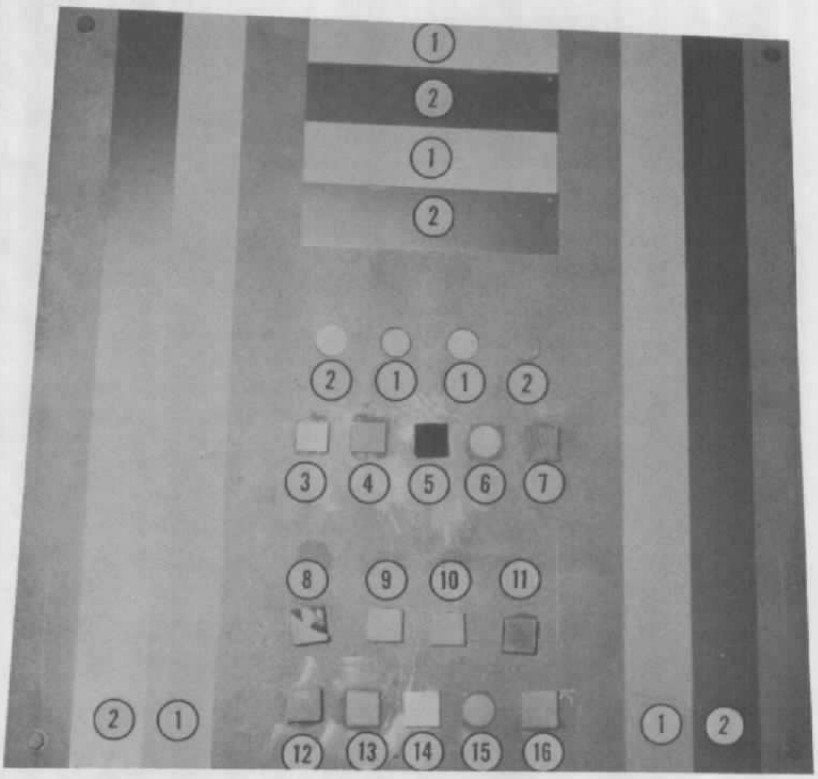

Specimen Identification	
1	Potassium silicate zinc oxide coating
2	Polyester, aluminum-pigmented paint
3	Aladine 407-41
4	Teflon spray on No. 170 Heatrem
5	SiO on aluminum on Schjeldahl tape
6	Checkerboard aluminum and ZnO paint in clear Heatrem binder
7	100-13 fiber glass cloth over aluminum foil
8	Oxalic acid on Apollo ablator material
9	Camphor coating over Saran Wrap on No. 170 Heatrem
10	Aladine 407-41 coated with camphor
11	Camphor and polyethylene on Apollo ablator material
12	Benzoic acid on Apollo ablator material
13	Camphor coating over SiO on aluminum on Schjeldahl tape
14	Saran Wrap on No. 170 Heatrem
15	Camphor coating over checkerboard aluminum and ZnO paint in clear Heatrem binder
16	Camphor coating over 100-13 fiber glass cloth over aluminum foil

b. Ablative Specimens

Fig. 8 Concluded

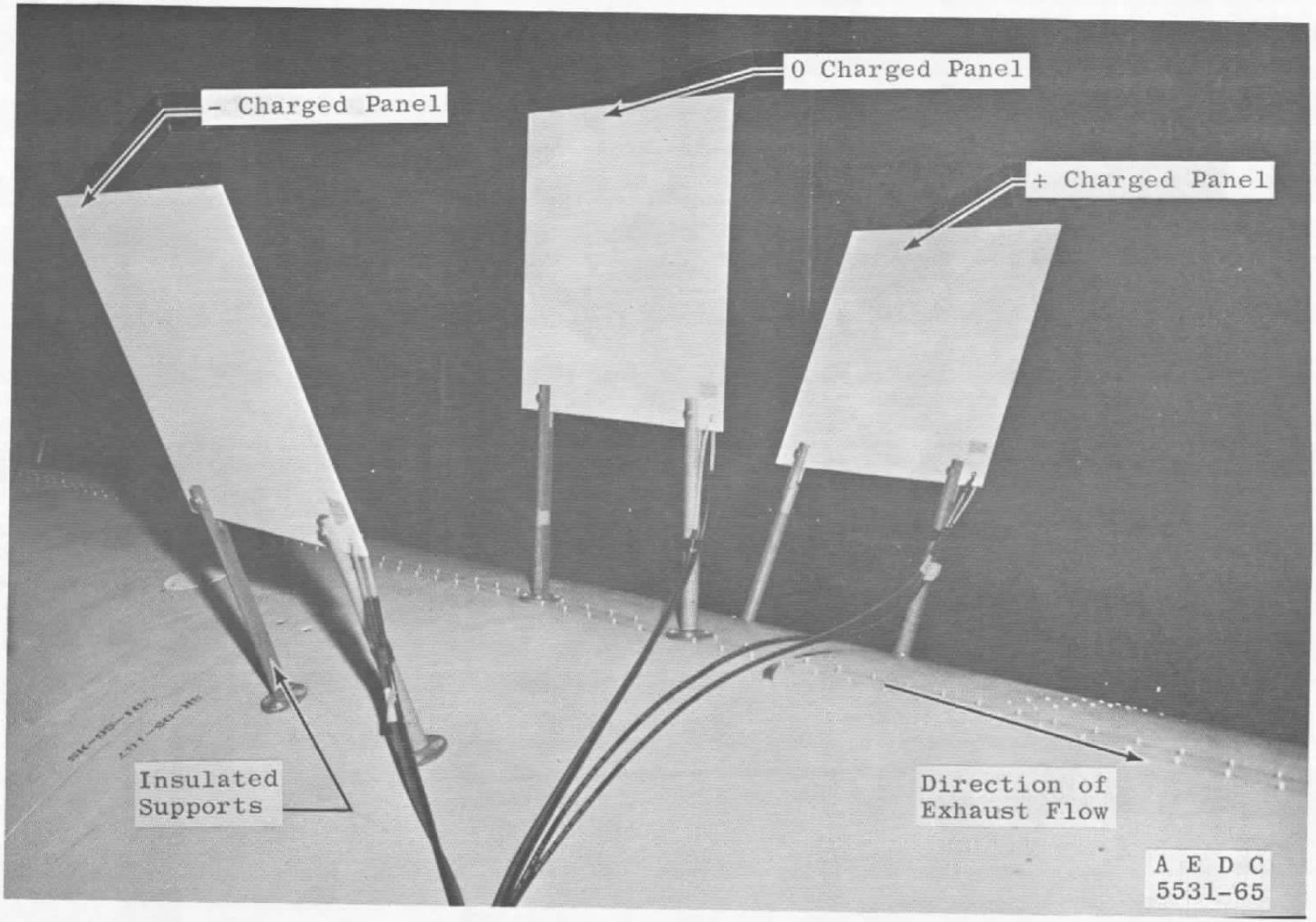

Fig. 9 Contamination Panel Configuration for the Charged Panel Experiment

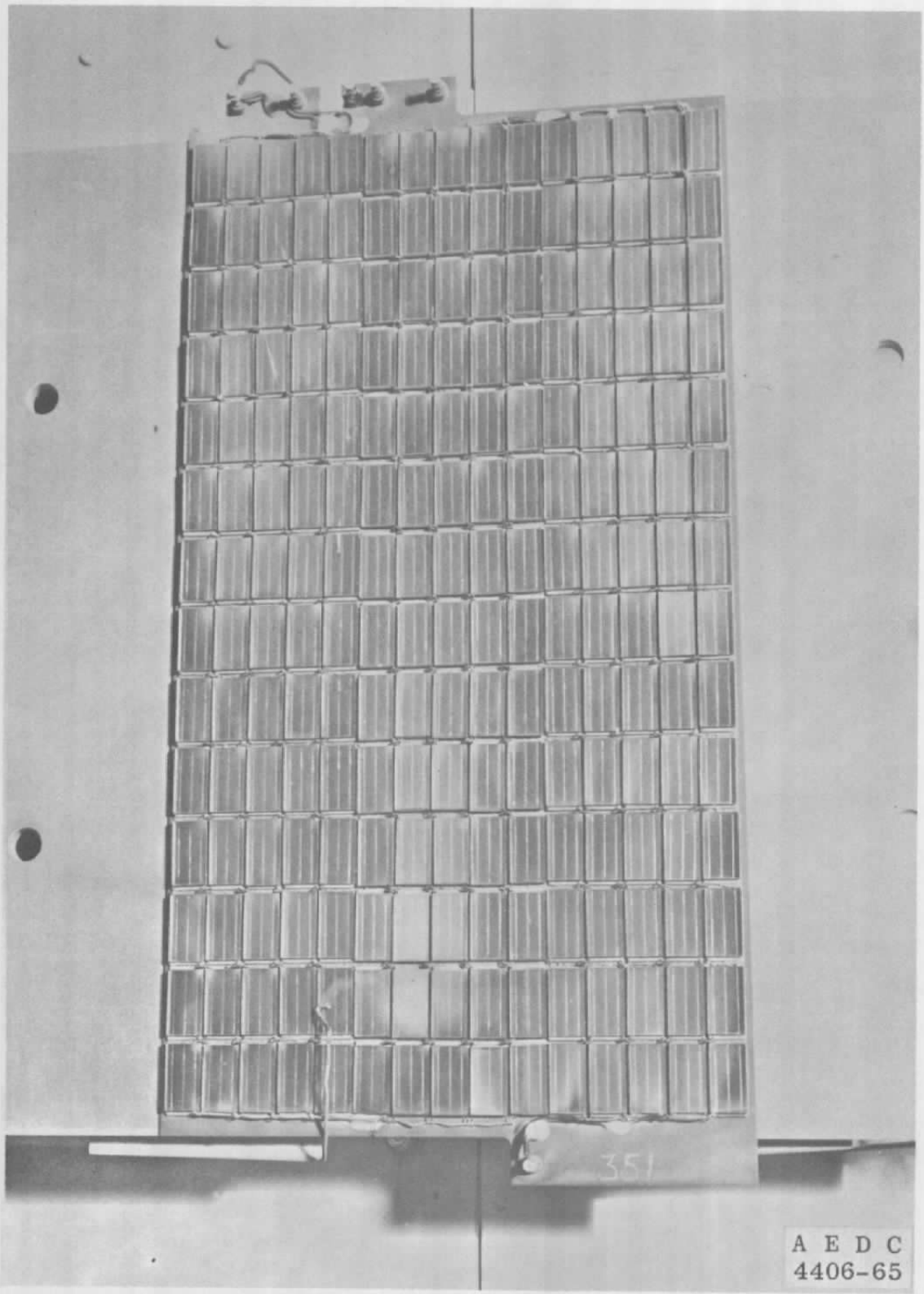

Fig. 10 Typical Solar Cell Panel

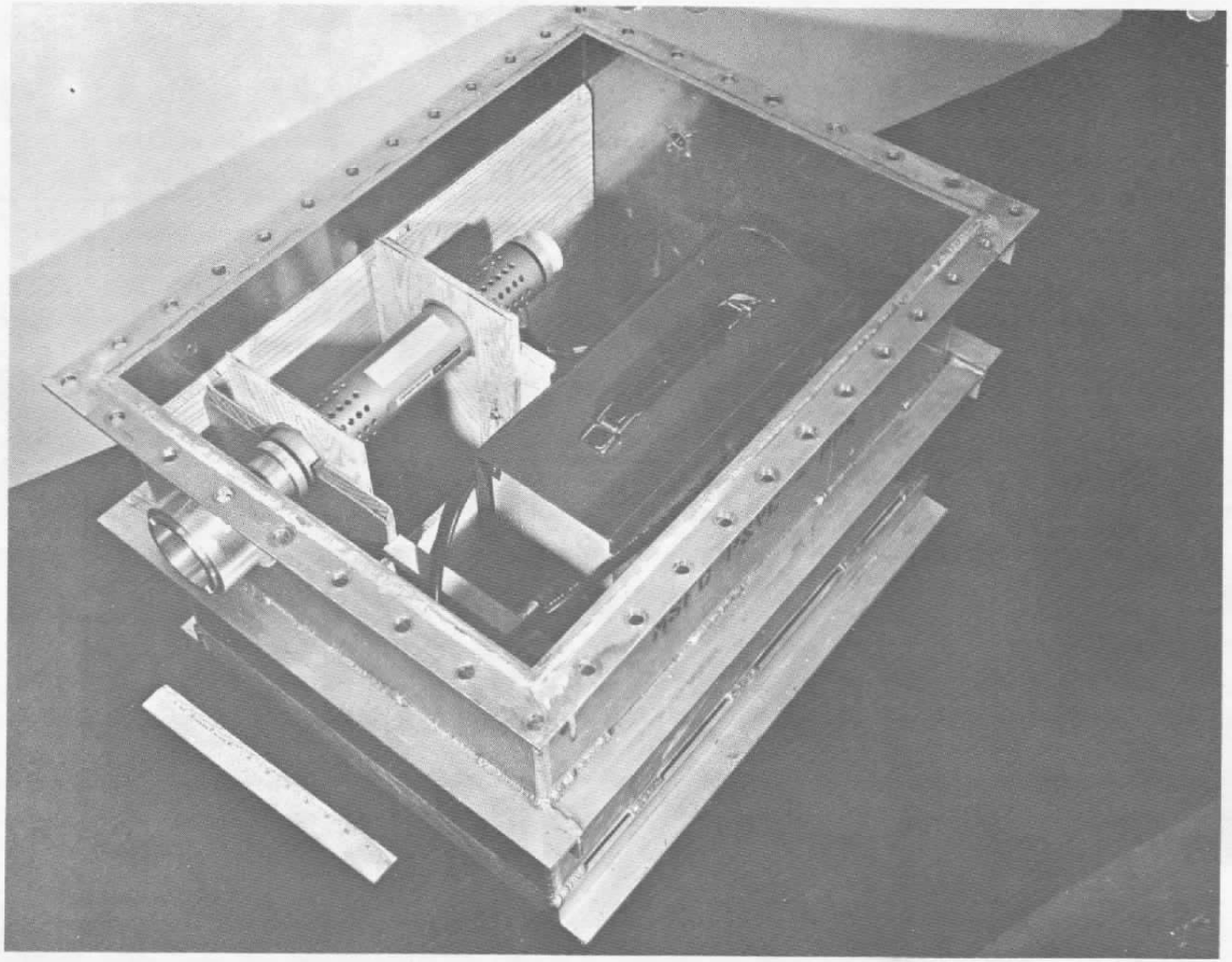

a. Perkin-Elmer Laser

Fig. 11 Helium-Neon Gas Laser Units

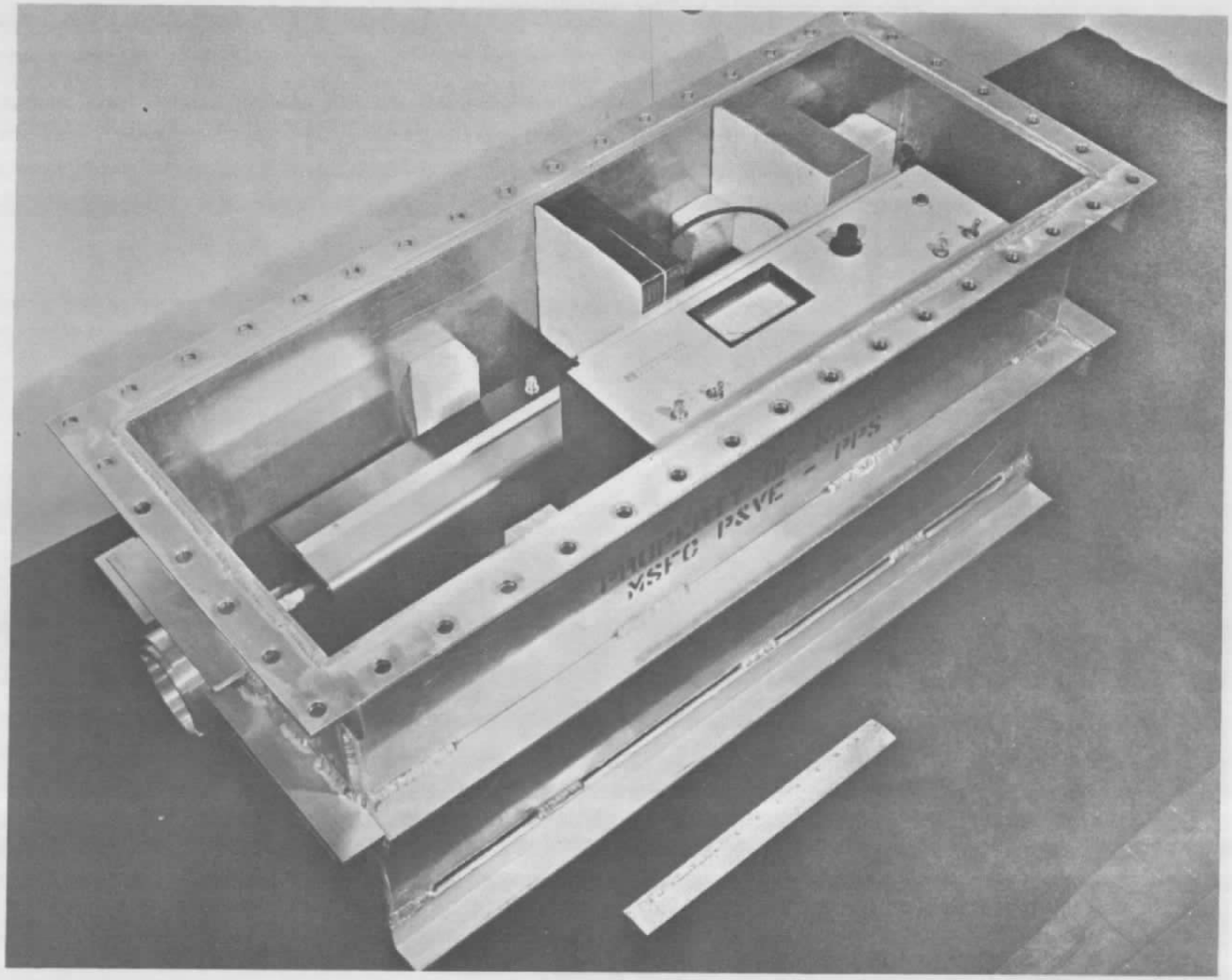

b. Spectra-Physics Laser

Fig. 11 Concluded

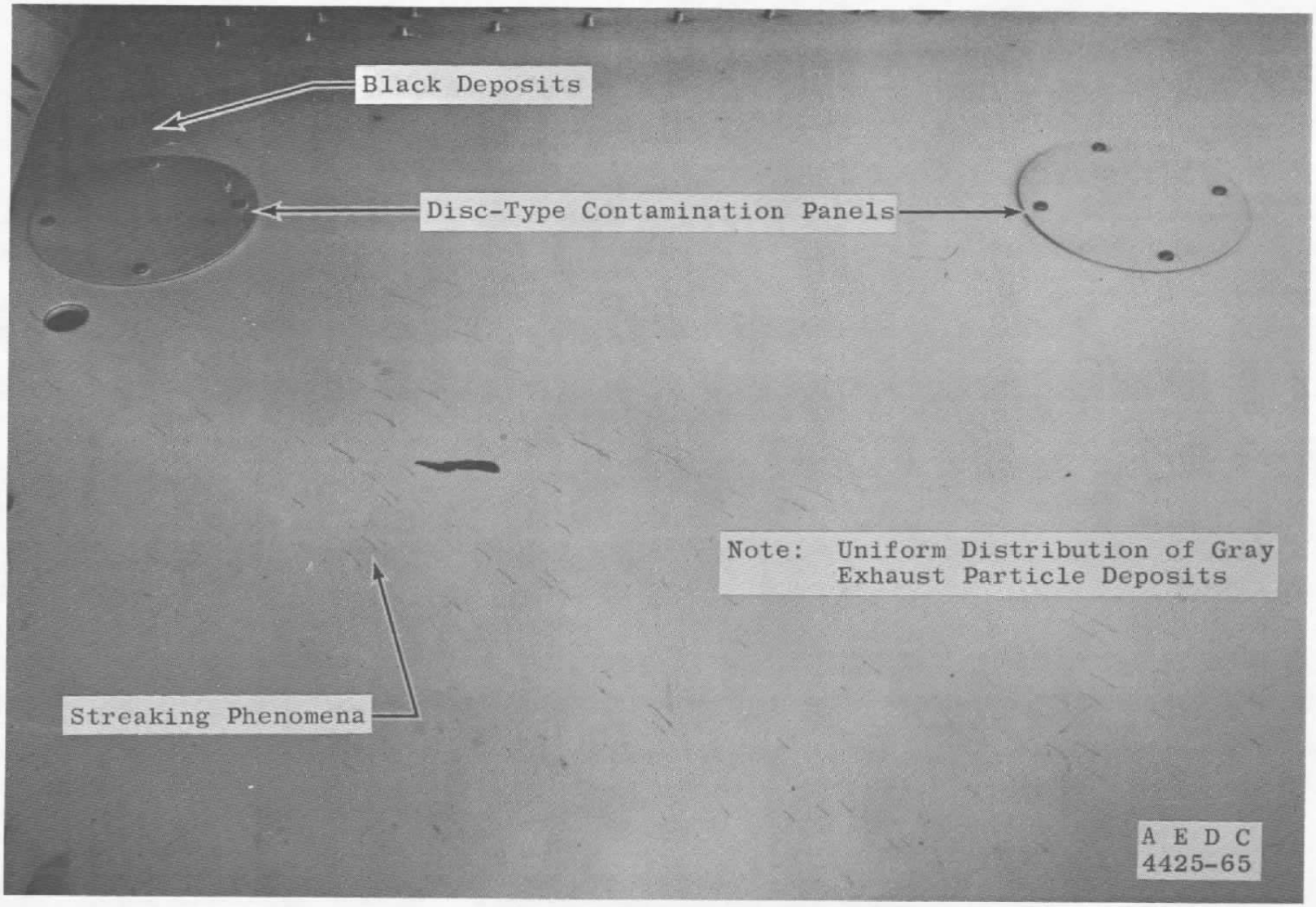

a. Model Surface

Fig. 12 Post-Fire Contamination Inspection

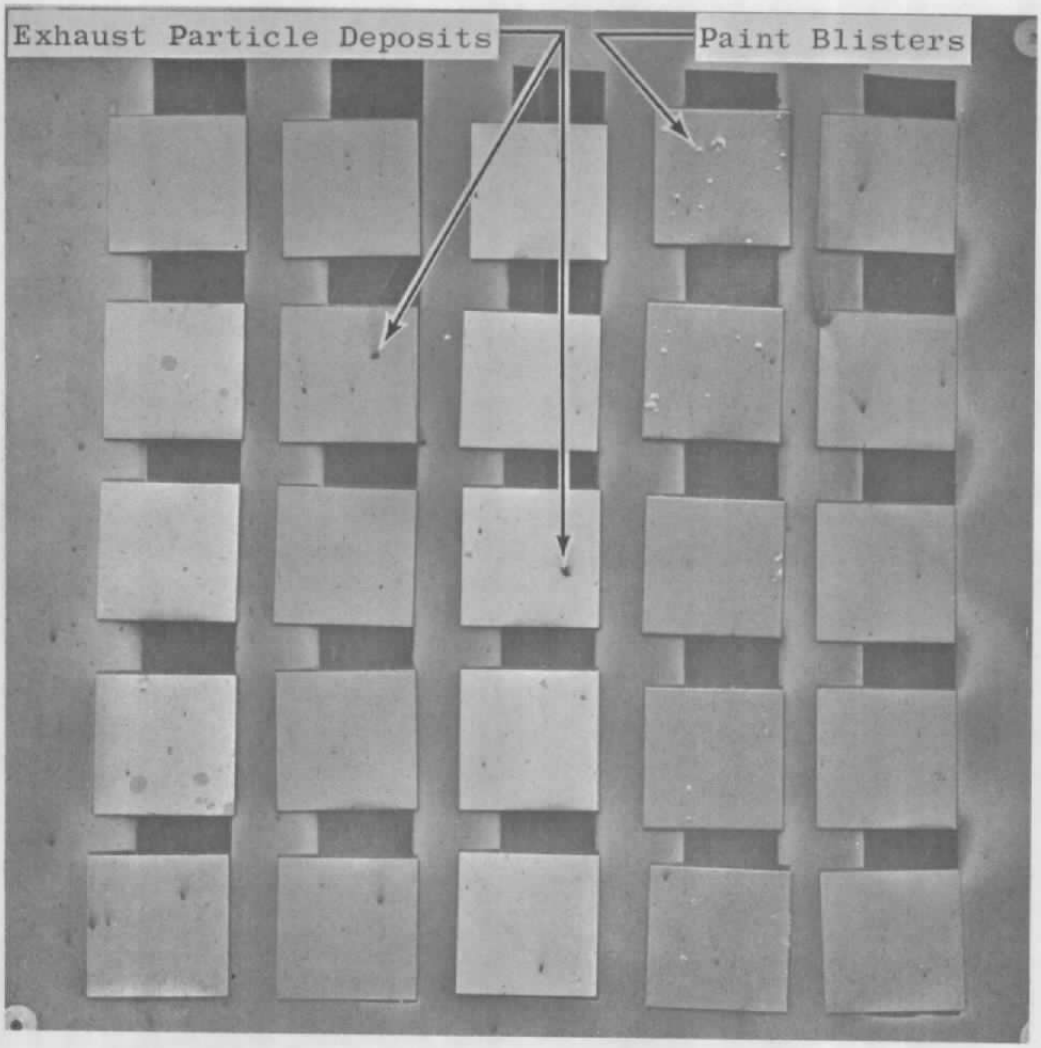

Column Number	Specimens
1	Insulfor Coating
2	$ZnCrO_4$ Primer
3	White Enamel
4	S-13 Paint
5	Bare Aluminum

b. Painted and Insulated Contamination Panel Specimens

Fig. 12 Continued

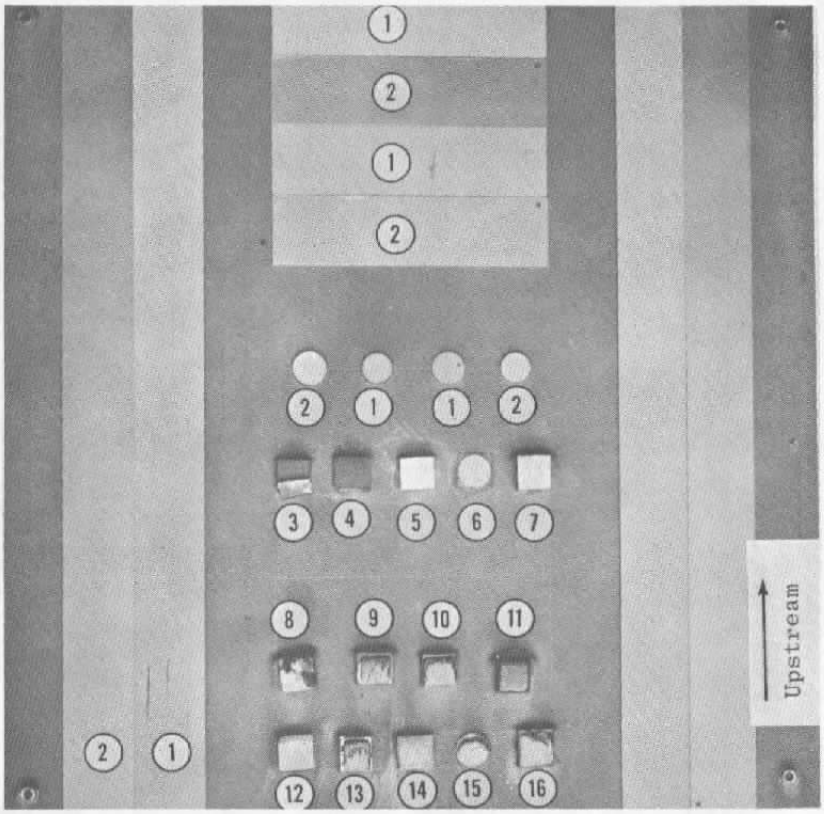

Specimen Identification	
1	Potassium silicate zinc oxide coating
2	Polyester, aluminum-pigmented paint
3	Aladine 407-41
4	Teflon spray on No. 170 Heatrem
5	SiO on aluminum on Schjeldahl tape
6	Checkerboard aluminum and ZnO paint in clear Heatrem binder
7	100-13 fiber glass cloth over aluminum foil
8	Oxalic acid on Apollo ablator material
9	Camphor coating over Saran Wrap on No. 170 Heatrem
10	Aladine 407-41 coated with camphor
11	Camphor and polyethylene on Apollo ablator material
12	Benzoic acid on Apollo ablator material
13	Camphor coating over SiO on aluminum on Schjeldahl tape
14	Saran Wrap on No. 170 Heatrem
15	Camphor coating over checkerboard aluminum and ZnO paint in clear Heatrem binder
16	Camphor coating over 100-13 fiber glass cloth over aluminum foil

c. Ablative Contamination Panel Specimens

Fig. 12 Concluded

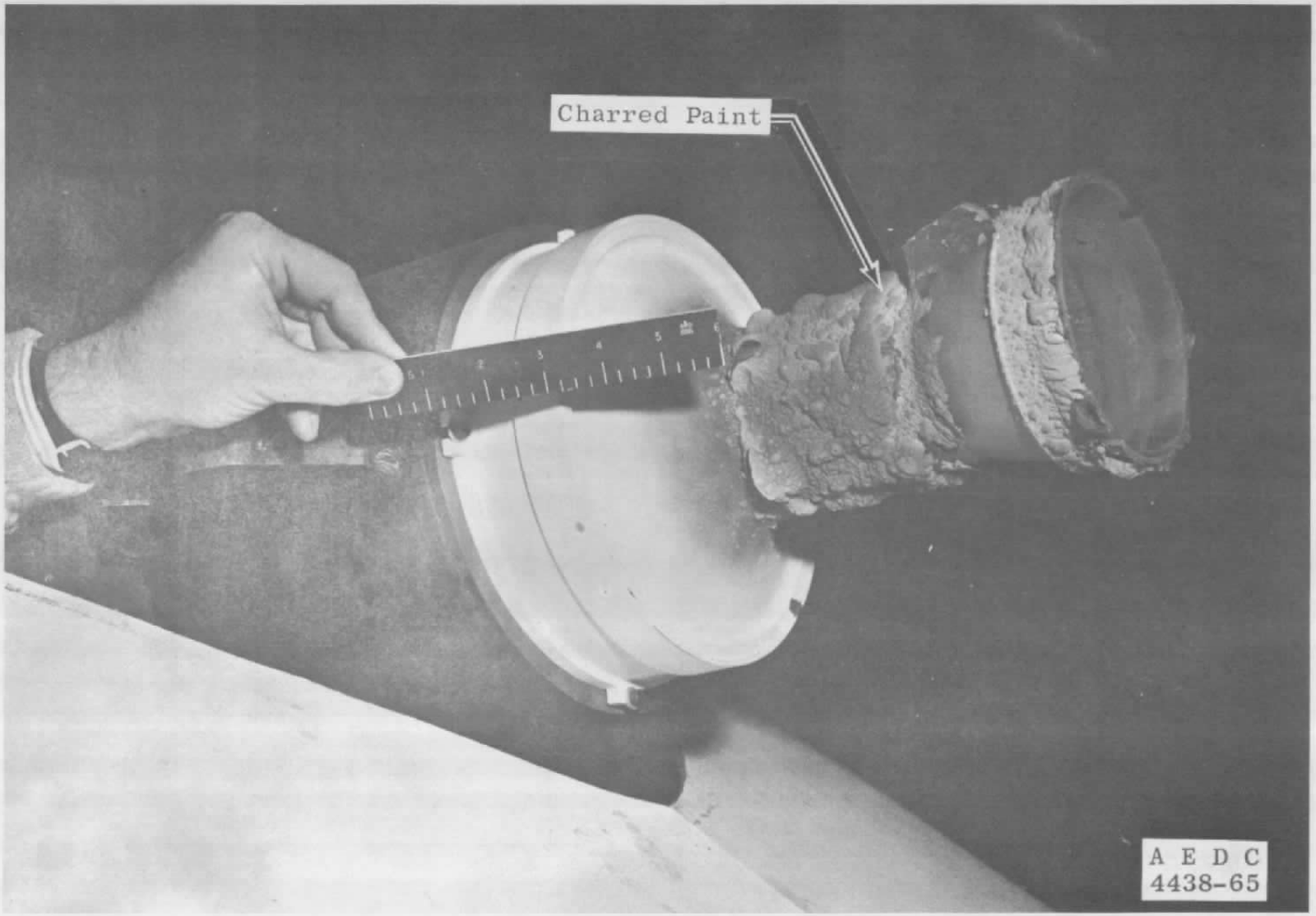

Fig. 13 S-IVB Retro Motor Nozzle Exit Cone, Post-Fire

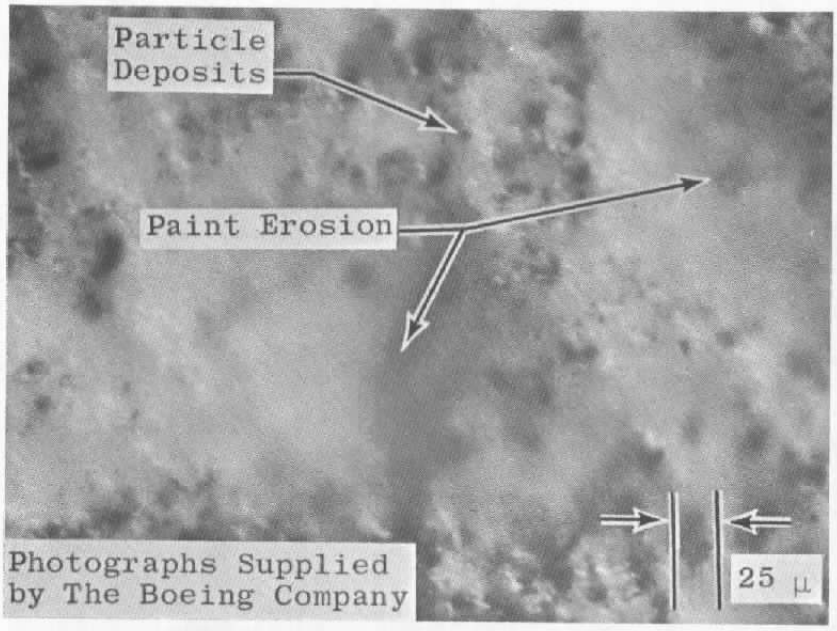

a. Exhaust Particle Clusters

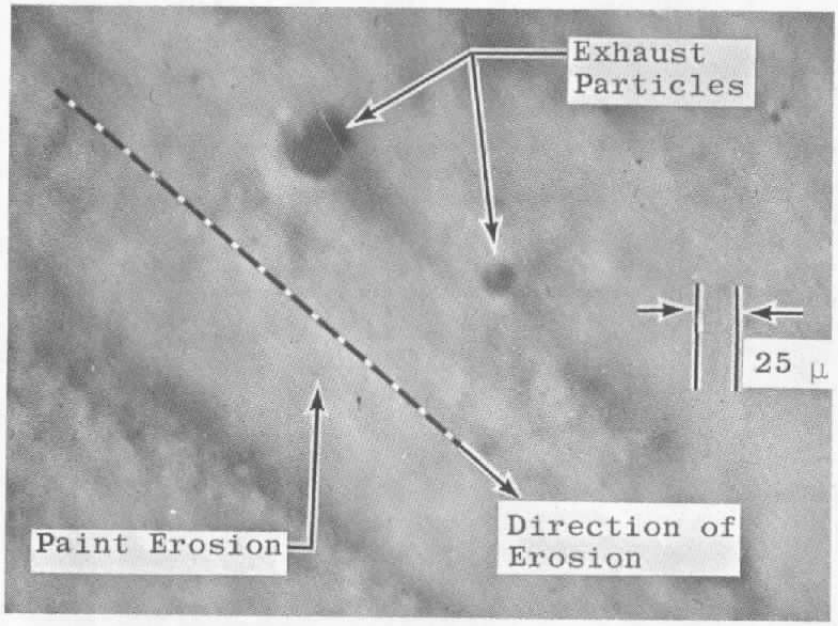

b. Exhaust Particles and Surface Erosion

Fig. 14 Typical Microscopic Inspection of Contamination Panels

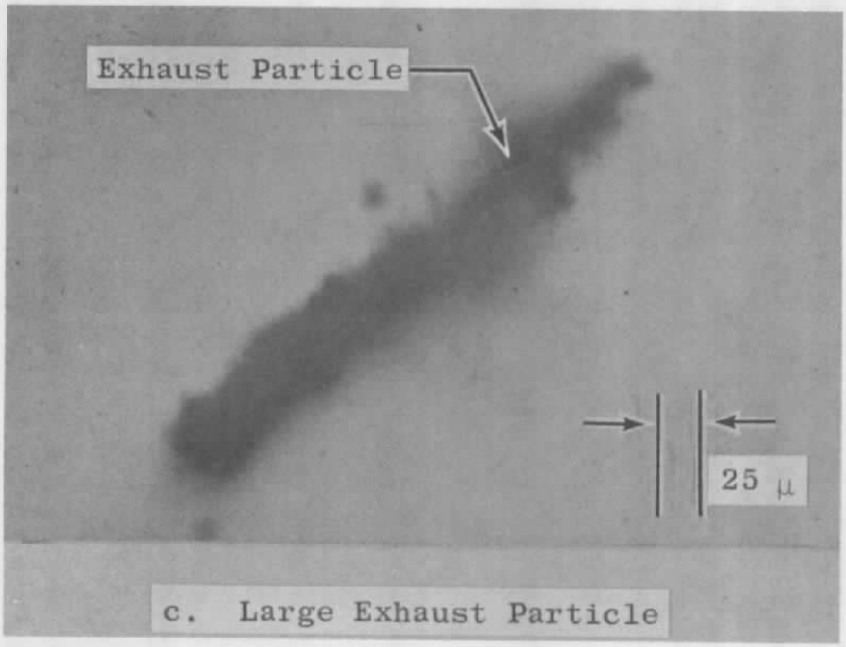

c. Large Exhaust Particle

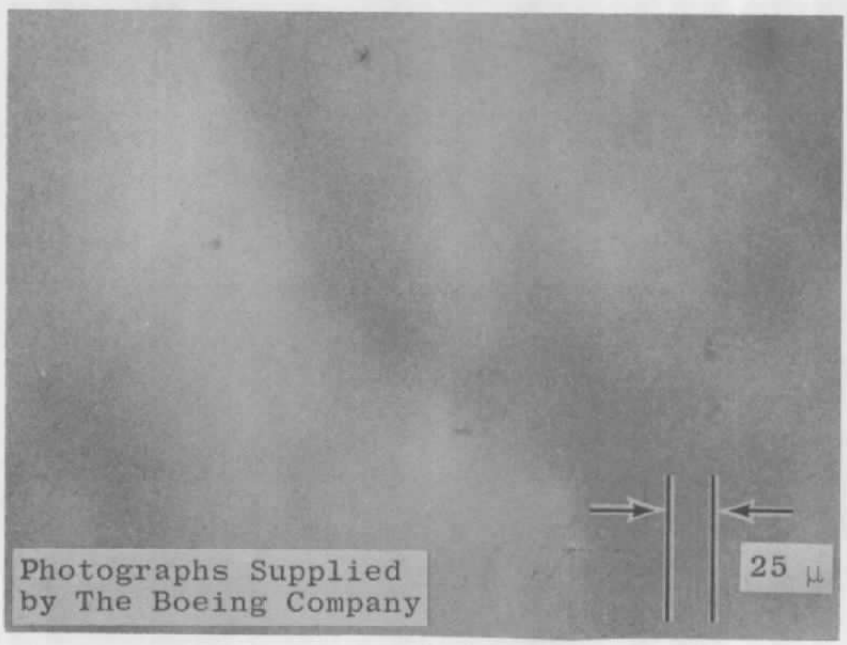

d. Panel Surface, Pre-Fire

Fig. 14 Concluded

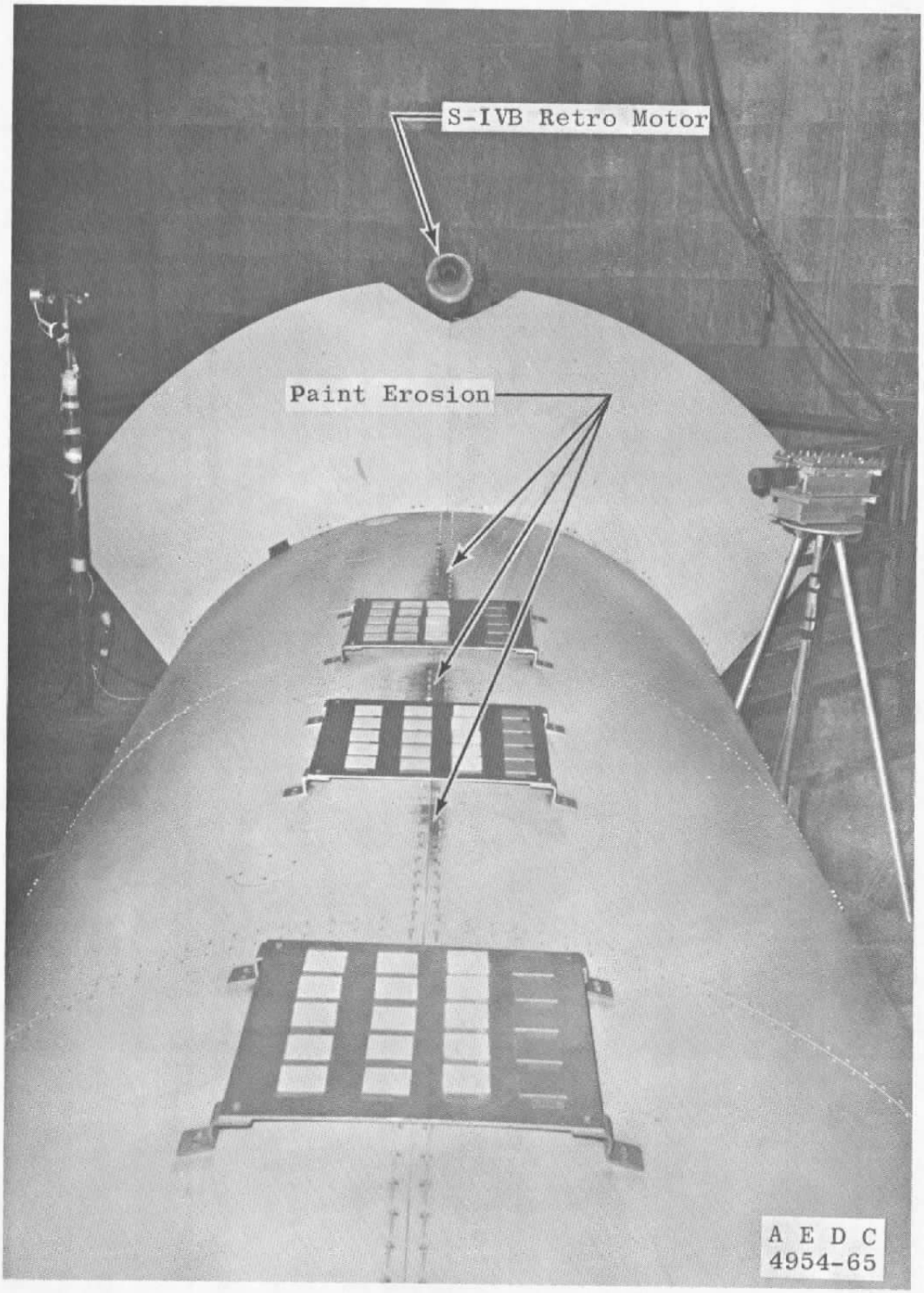

Fig. 15 Model Surface Paint Erosion

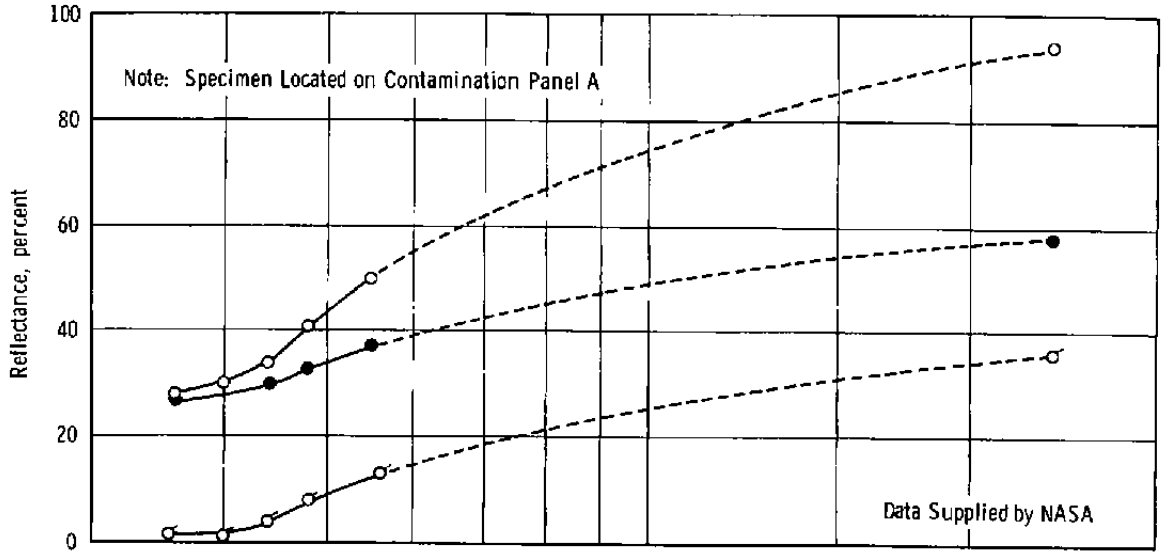

a. Bare Aluminum Specimen

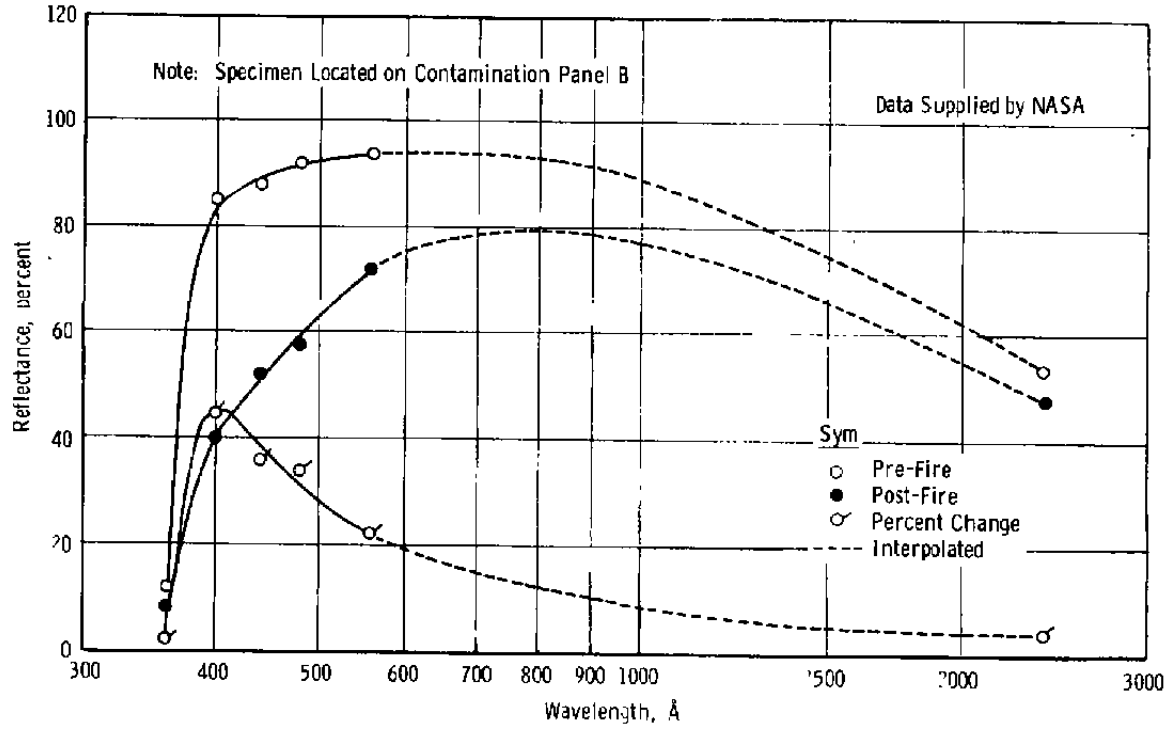

b. S-13 Paint Specimen

Fig. 16 Surface Reflectance of Various Contamination Specimens

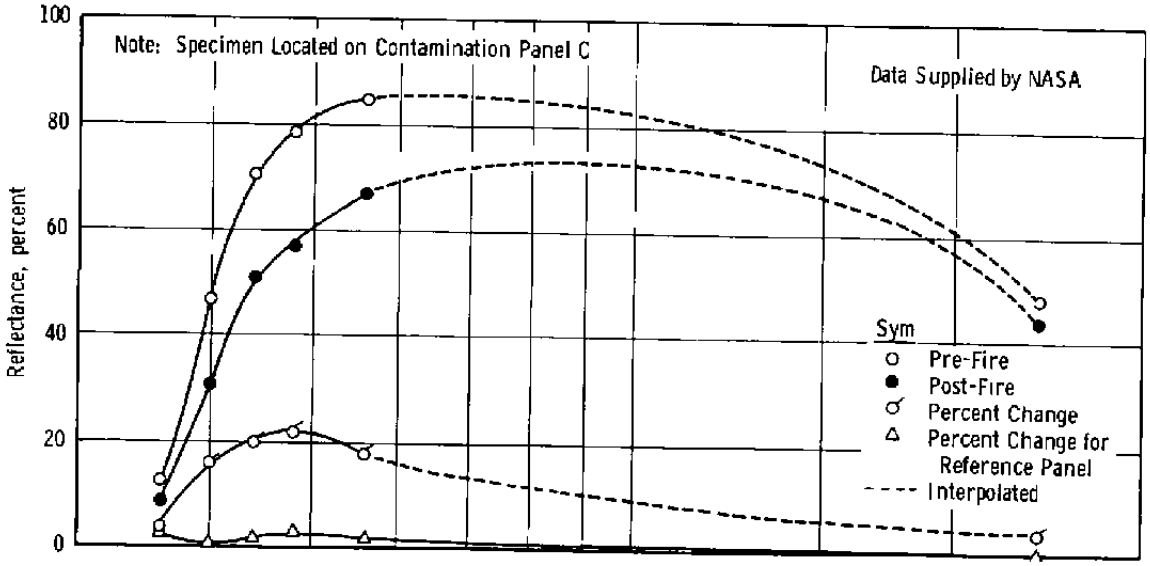

c. White Enamel Specimen

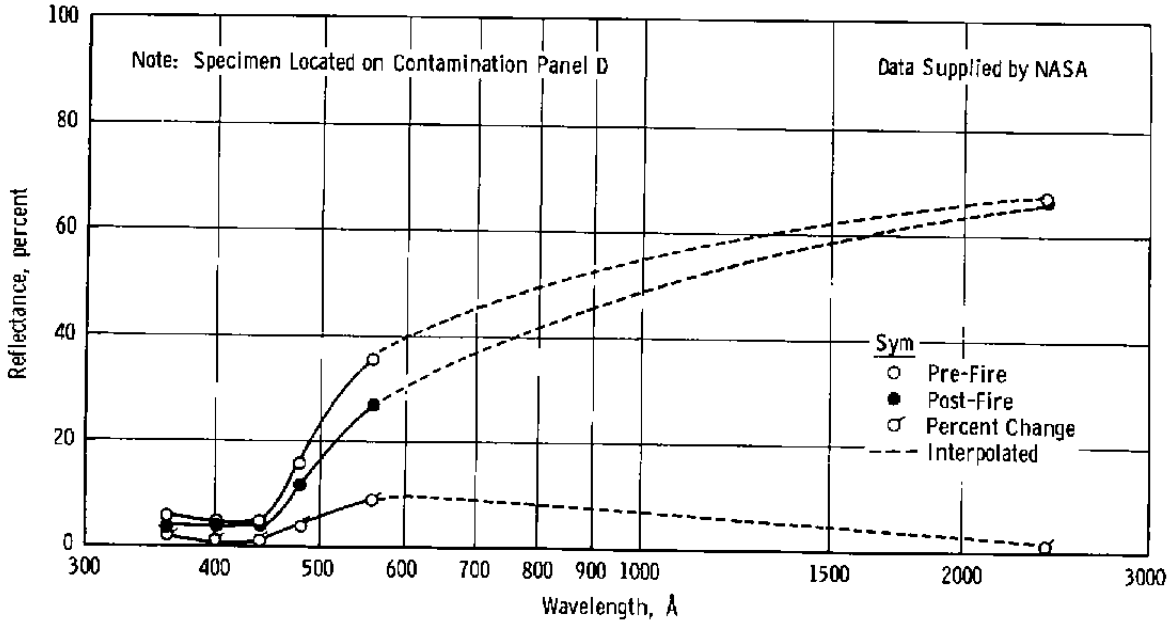

d. Zinc Chromate Specimen

Fig. 16 Continued

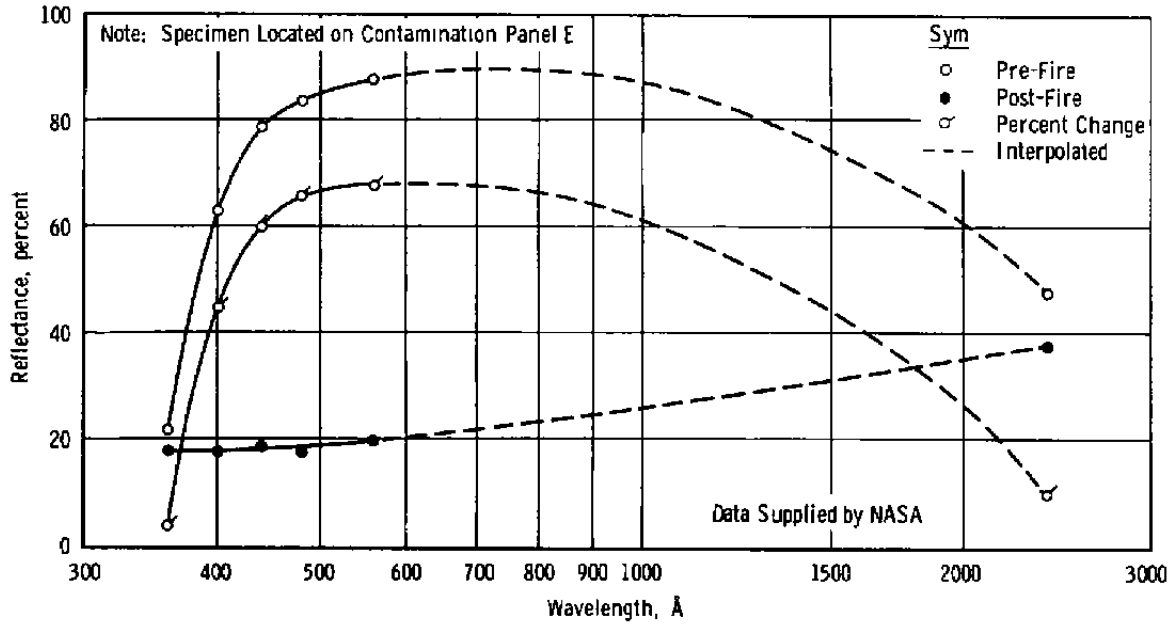

e. Insulfor Specimen

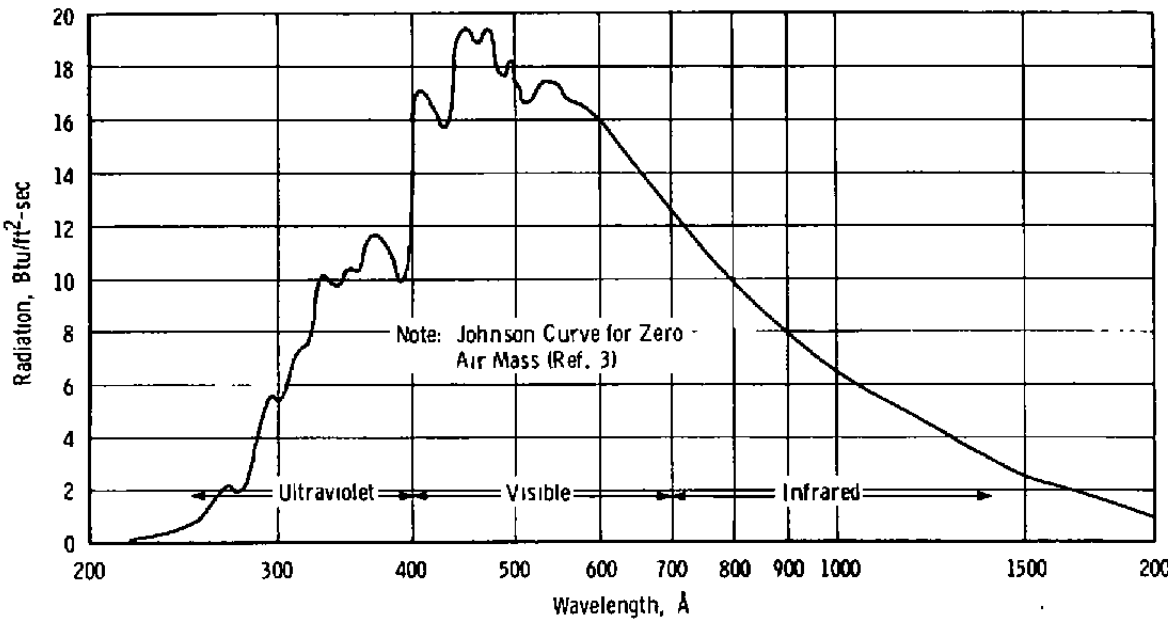

f. Solar Spectral-Irradiance

Fig. 16 Concluded

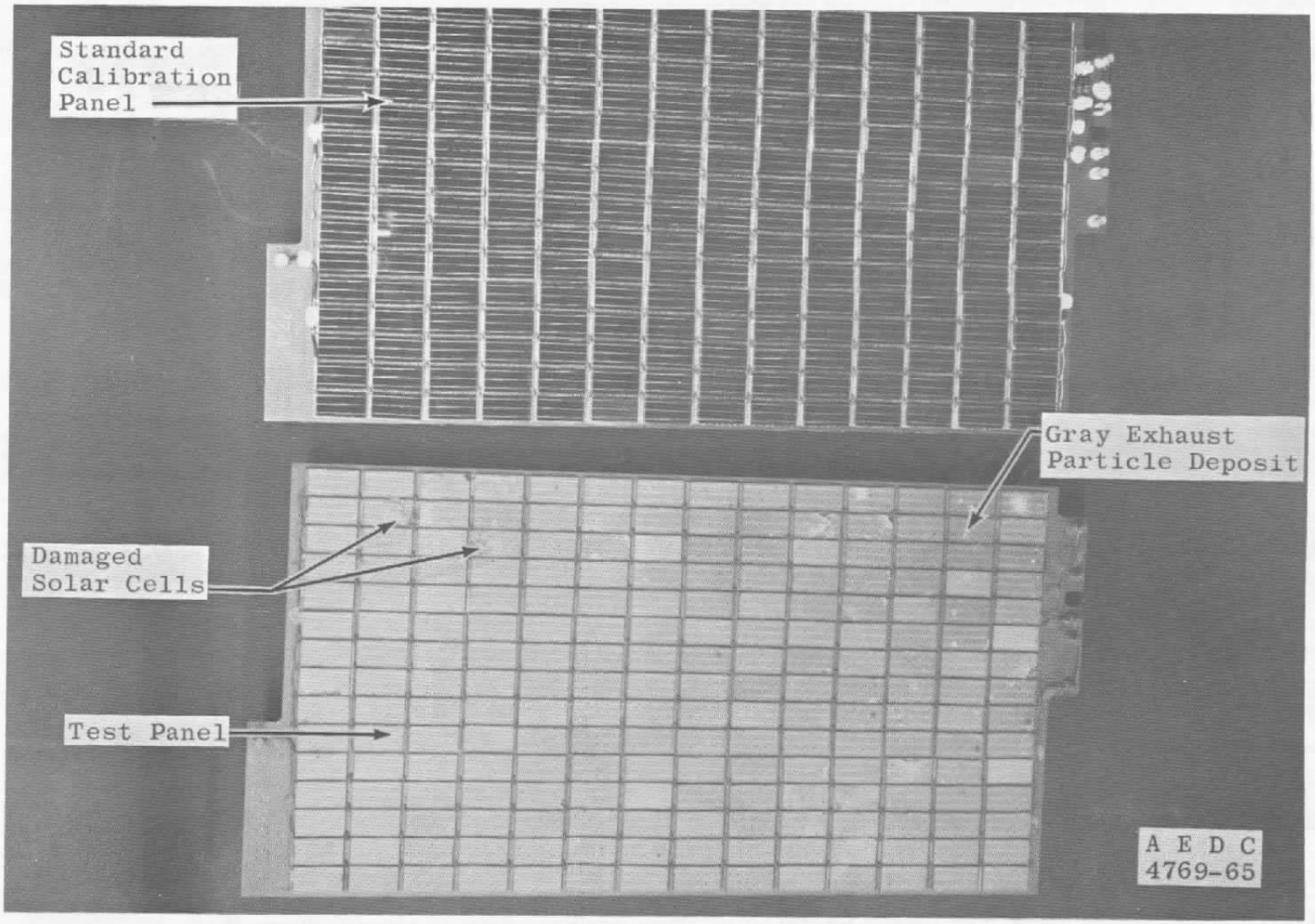

Fig. 17 Solar Cell Panel Degradation

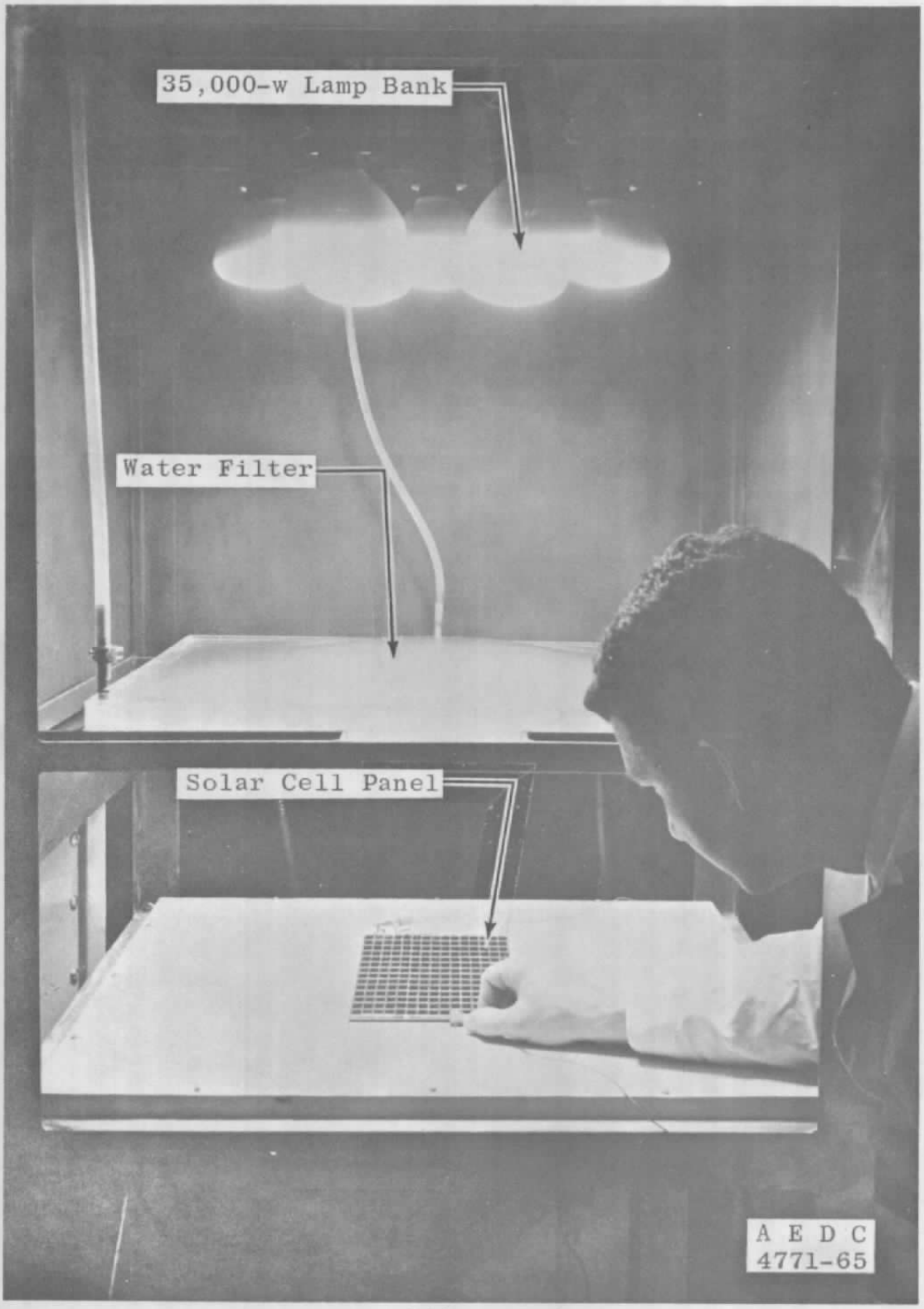

a. Calibration Rack

Fig. 18 Solar Cell Panel Calibration

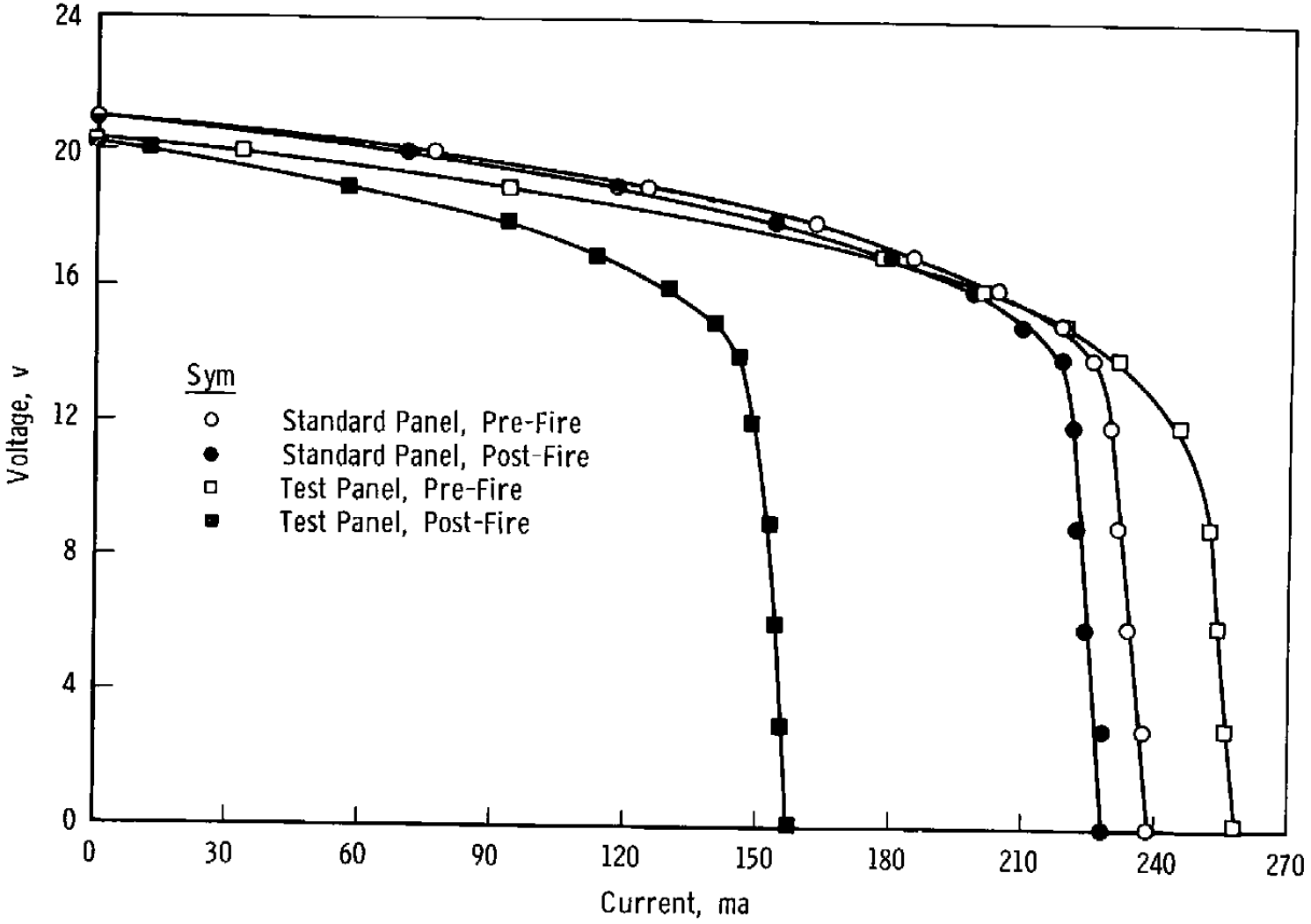

b. Typical Calibration Curves

Fig. 18 Concluded

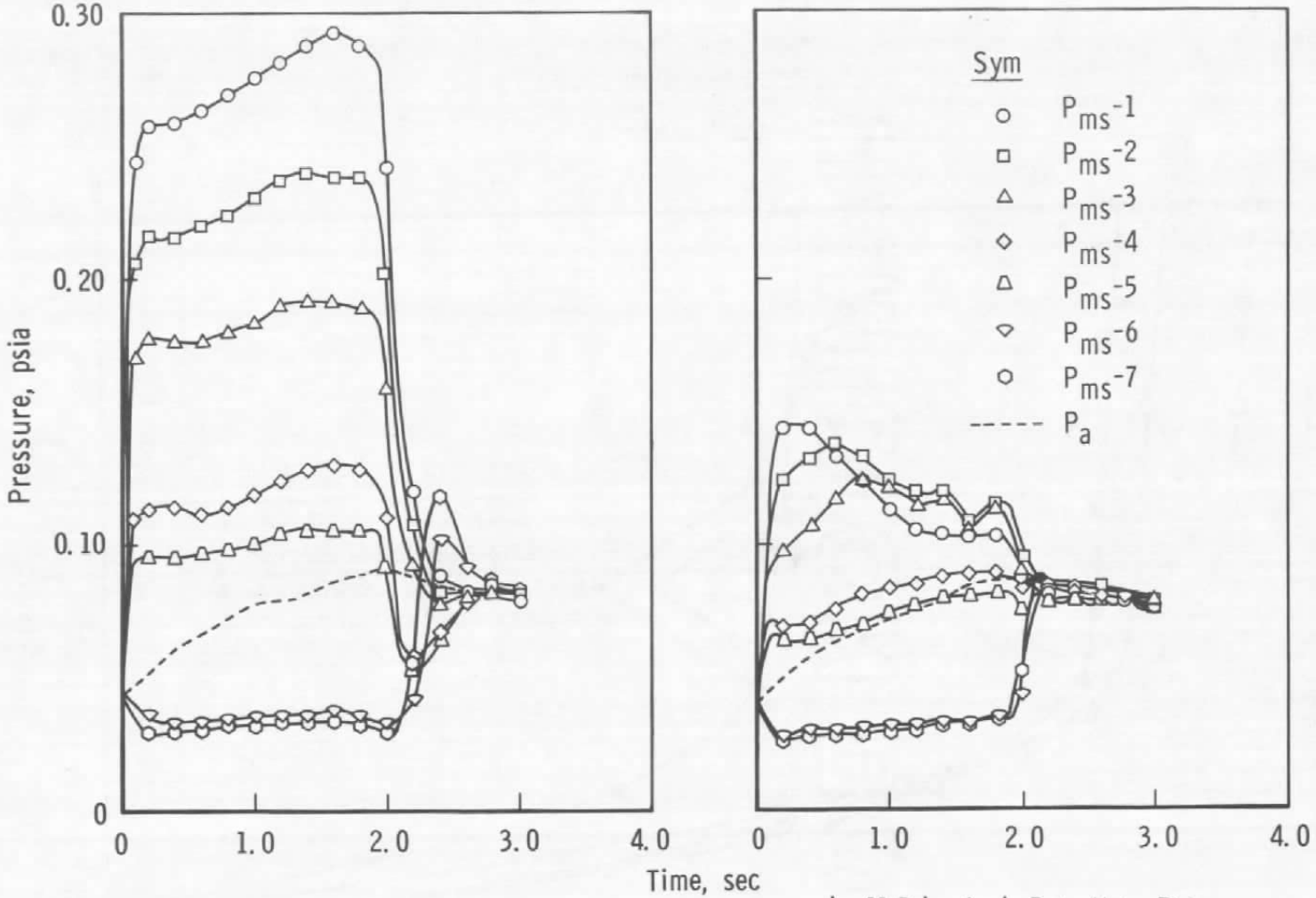

a. 0-deg Angle Retro Motor Firing

b. 11.5-deg Angle Retro Motor Firing

Fig. 19 Typical Model Surface Pressure Distribution

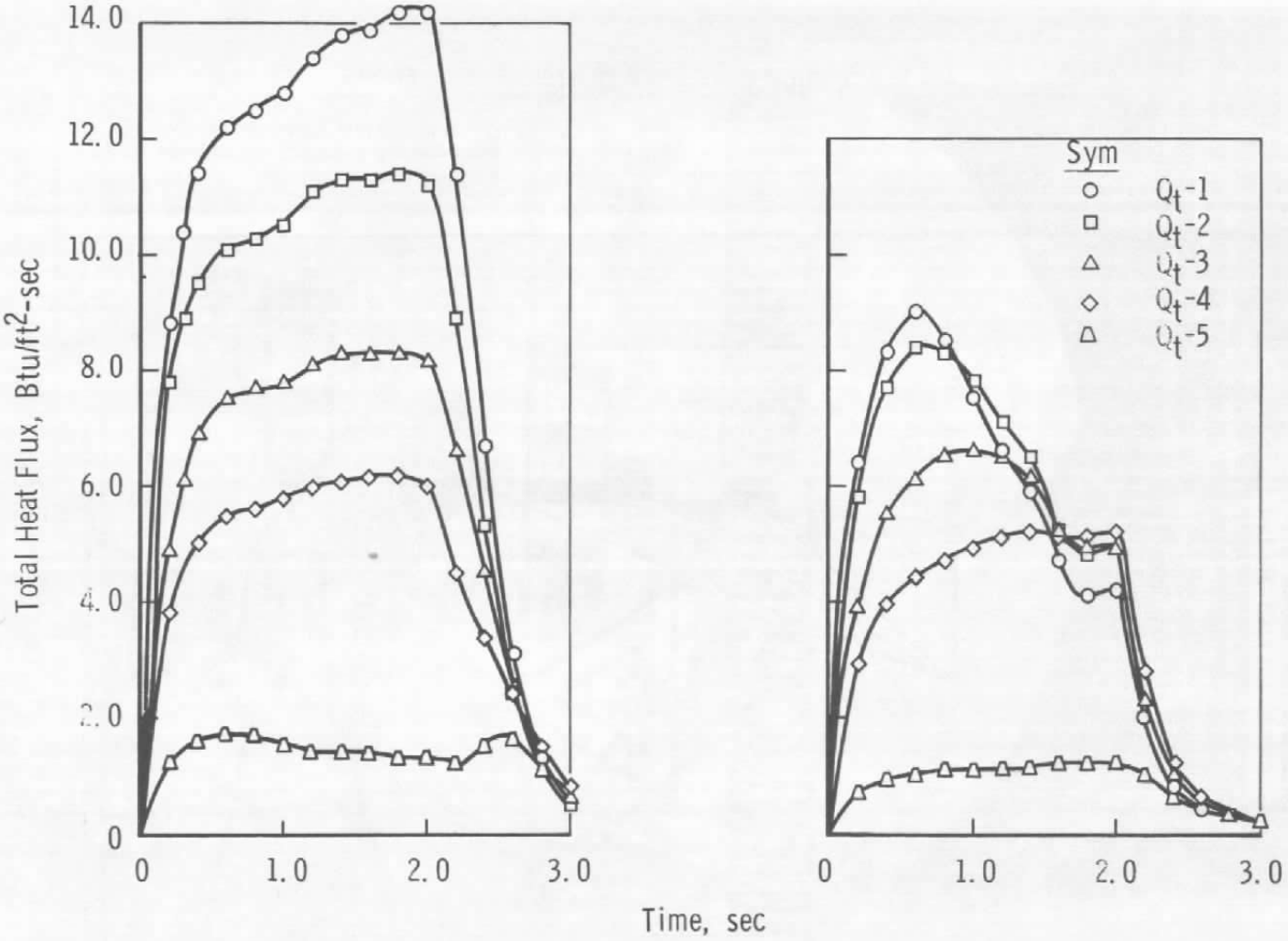

a. 0-deg Angle Retro Motor Firing

b. 11.5-deg Angle Retro Motor Firing

Fig. 20 Typical Model Surface Heating Rate Distribution

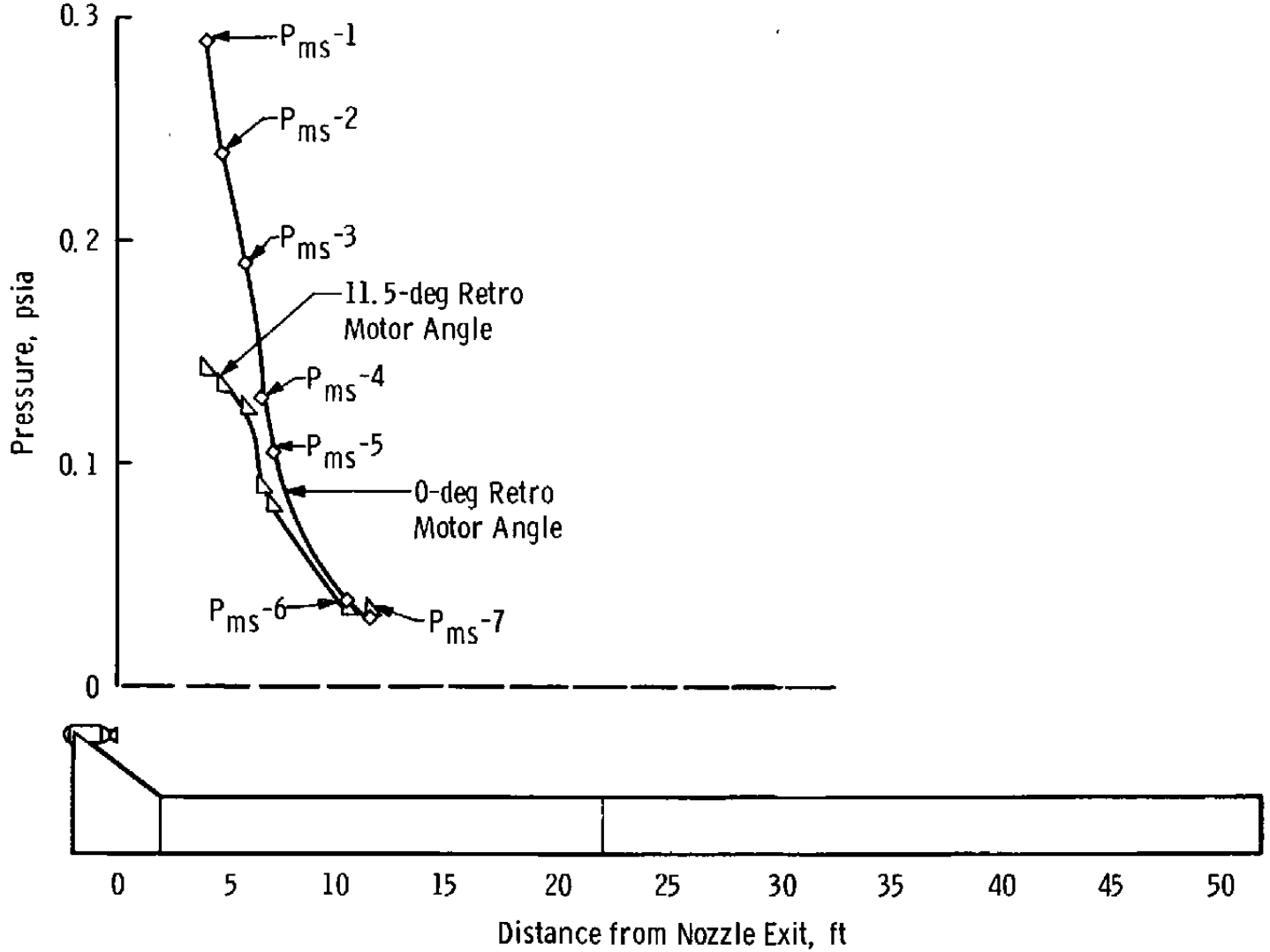

Fig. 21 Typical Profile of Maximum Model Surface Pressures

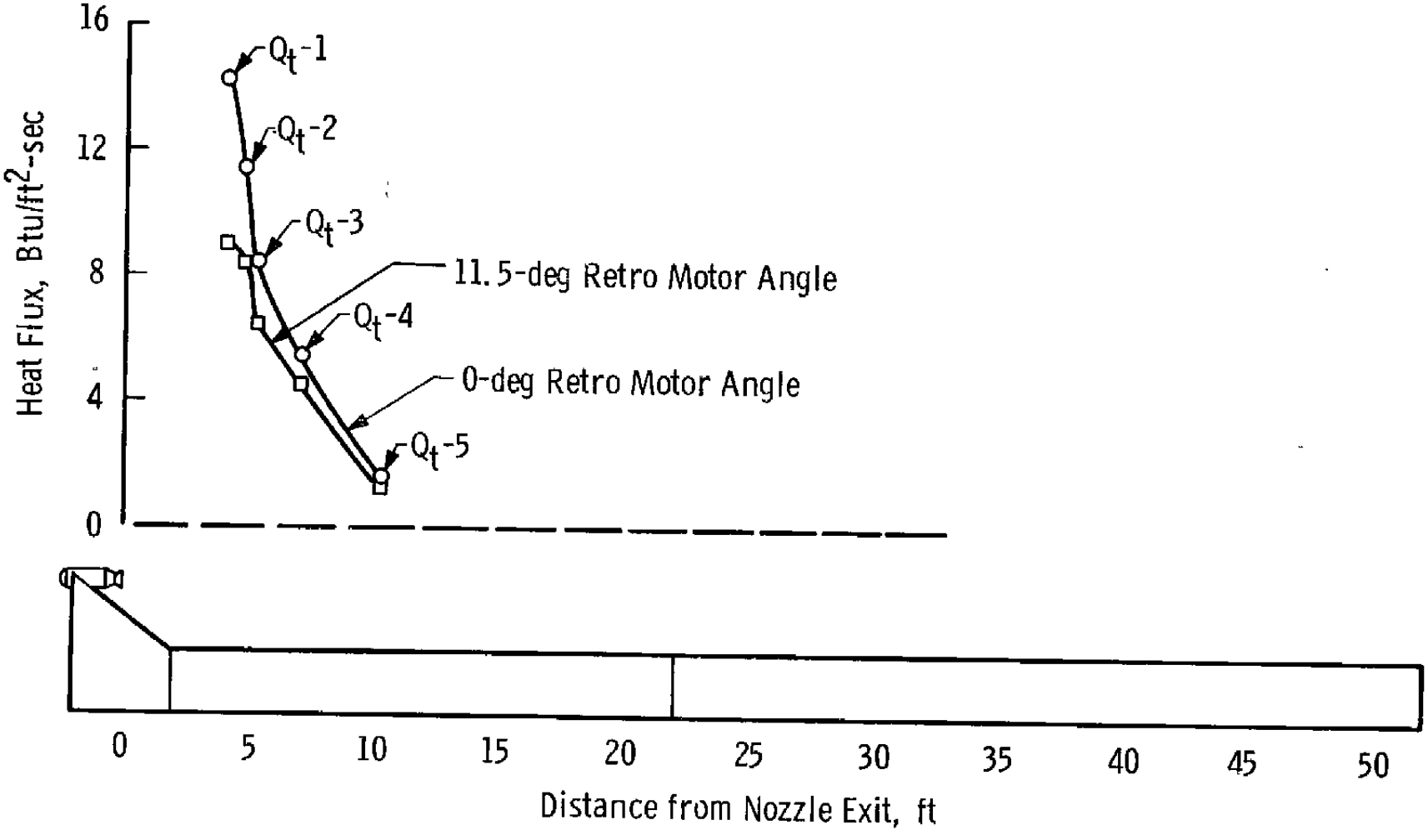

Fig. 22 Typical Profile of Maximum Model Surface Heating Rates

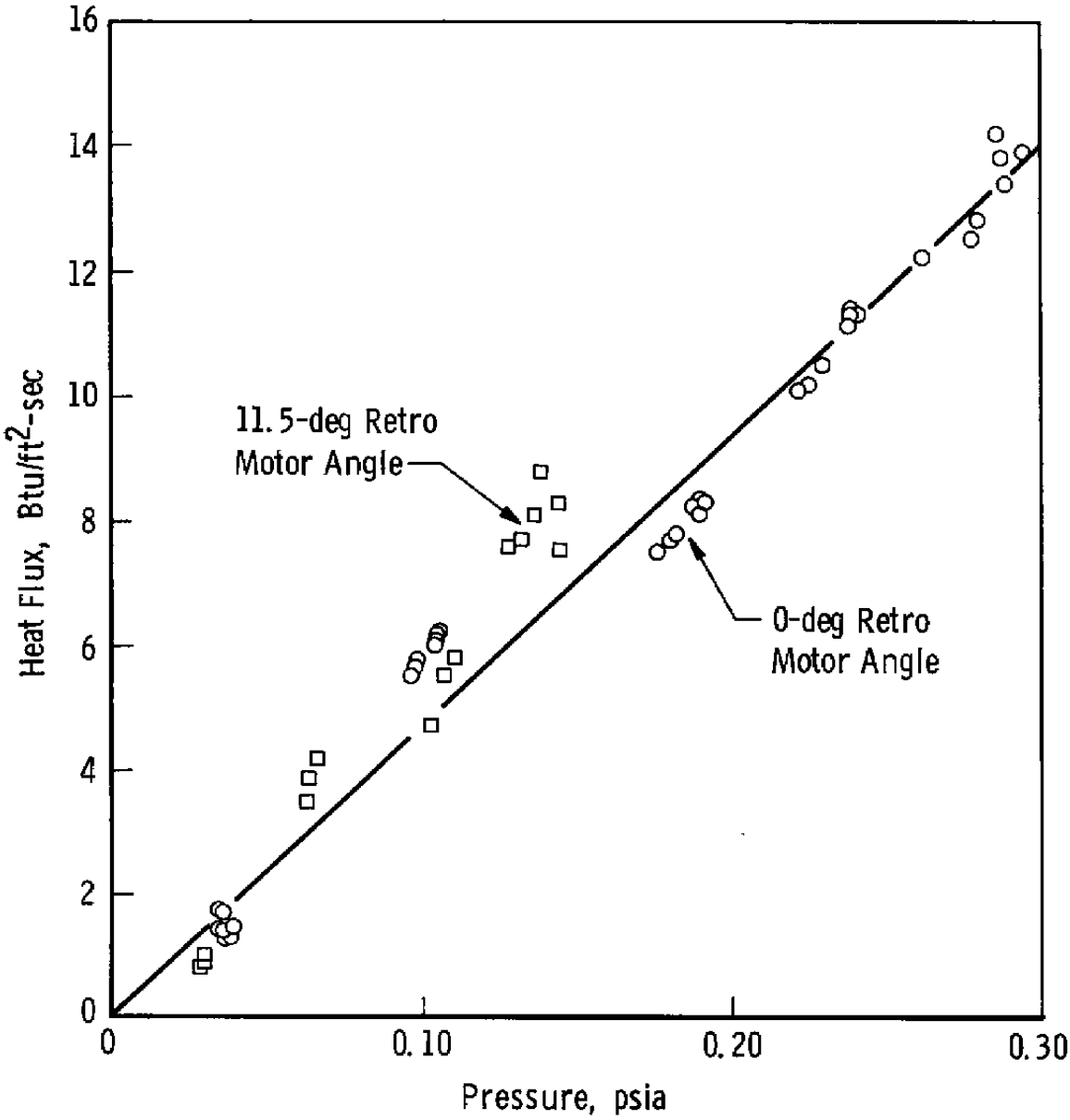

Fig. 23 Model Surface Pressure and Heating Rate Relationship

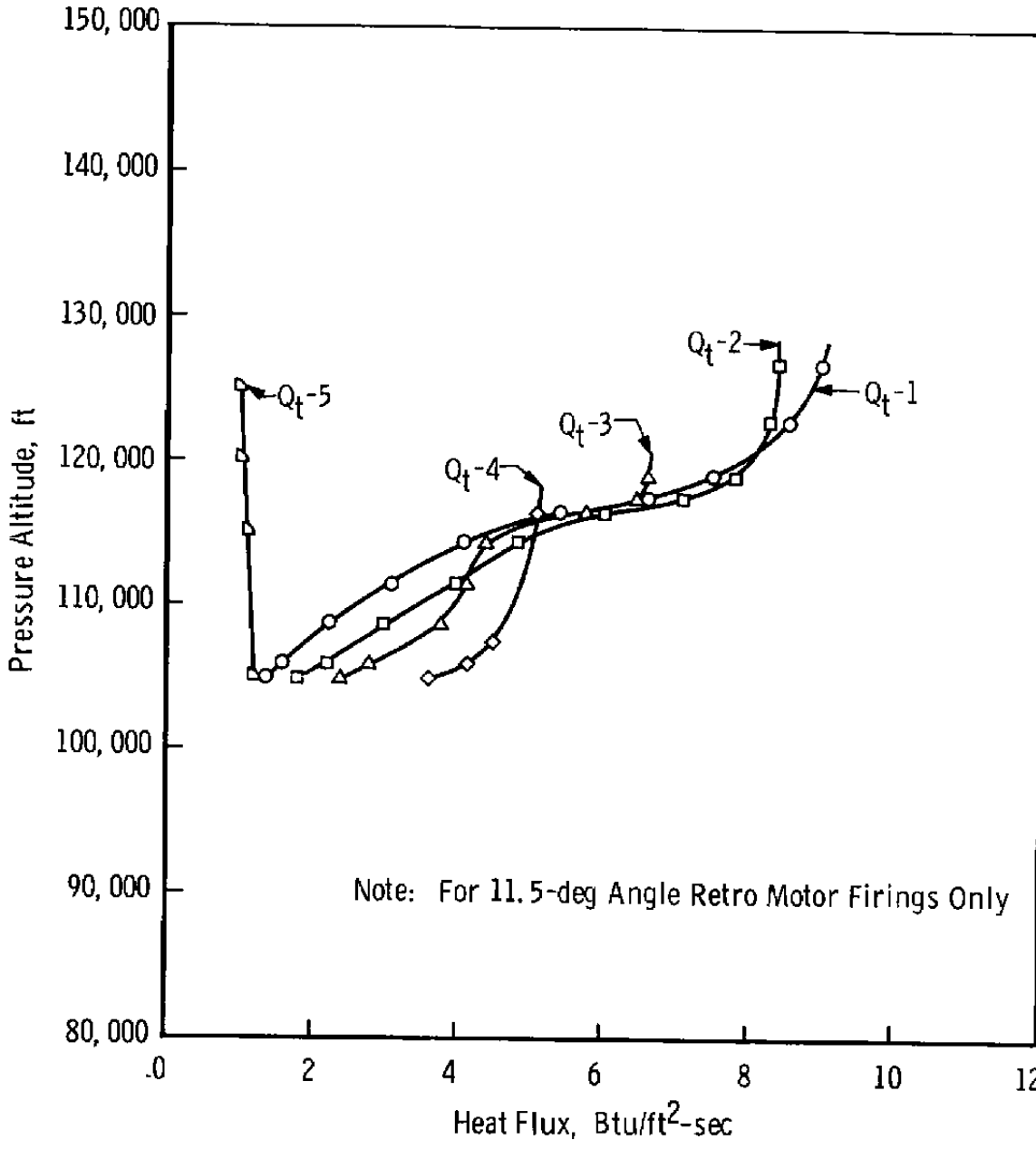

Fig. 24 Altitude Effect on Model Surface Heating Rates

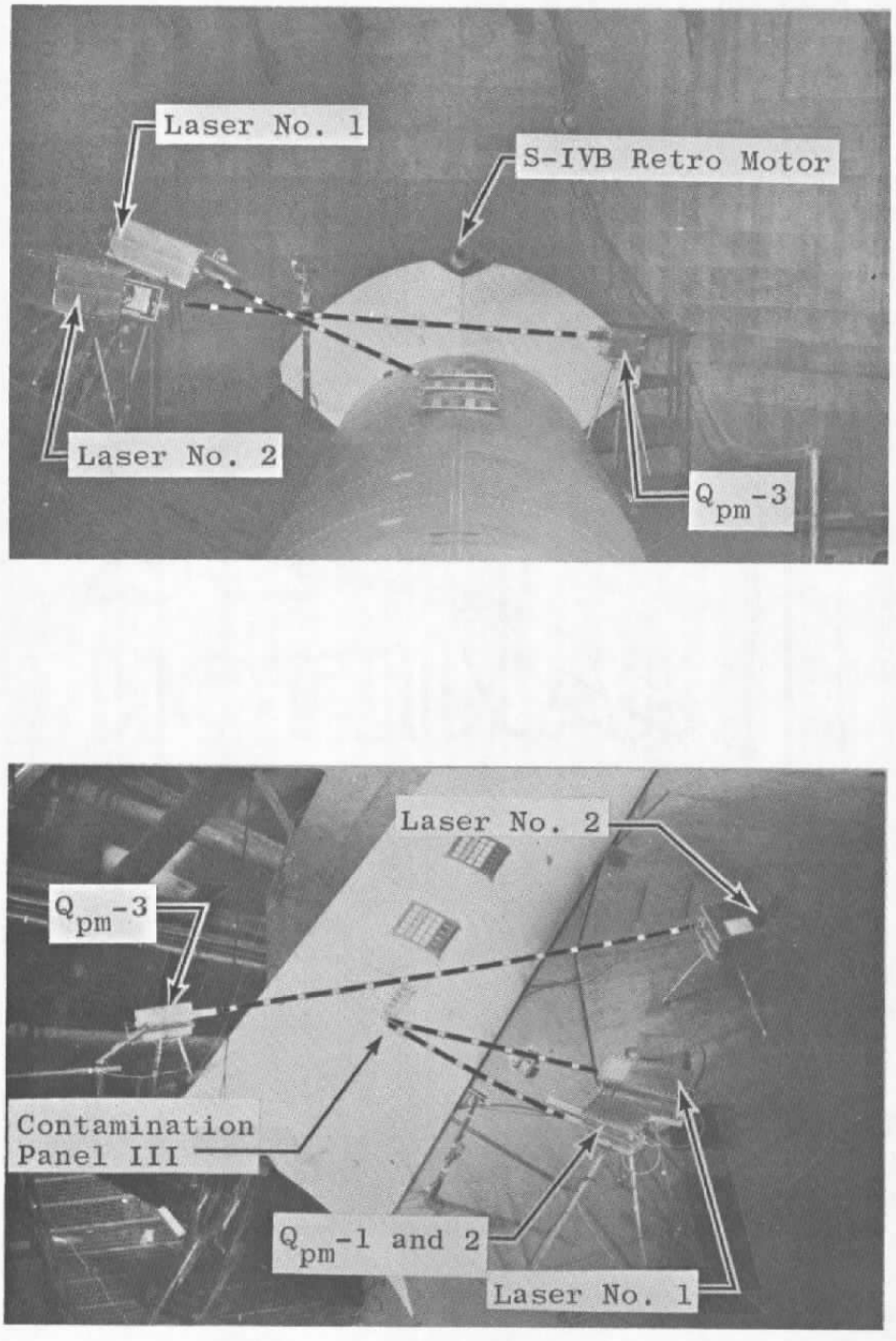

Fig. 25 Test Equipment Setup for Laser Experiments

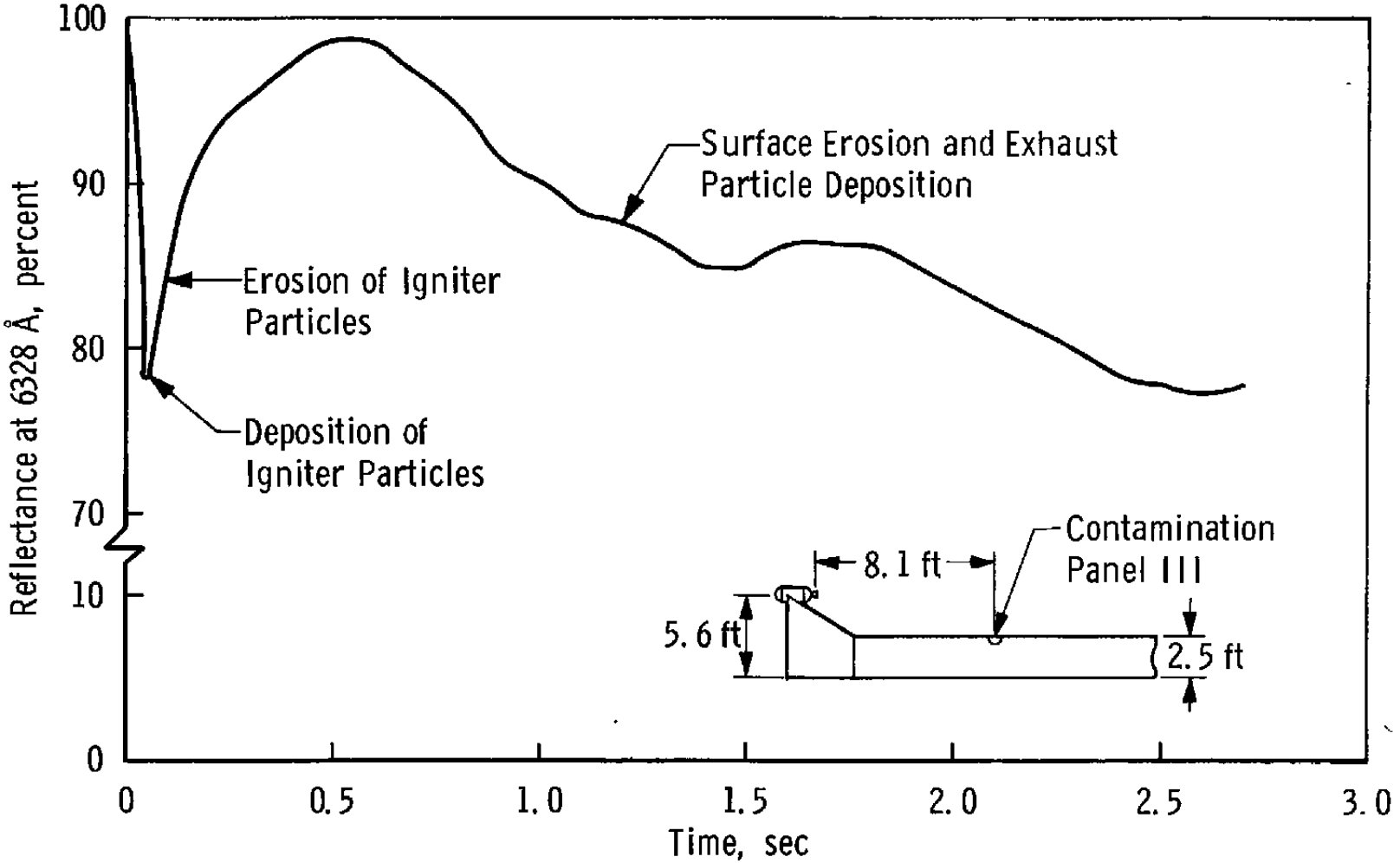

Fig. 26 Contamination Panel III Reflectance of a Laser Beam

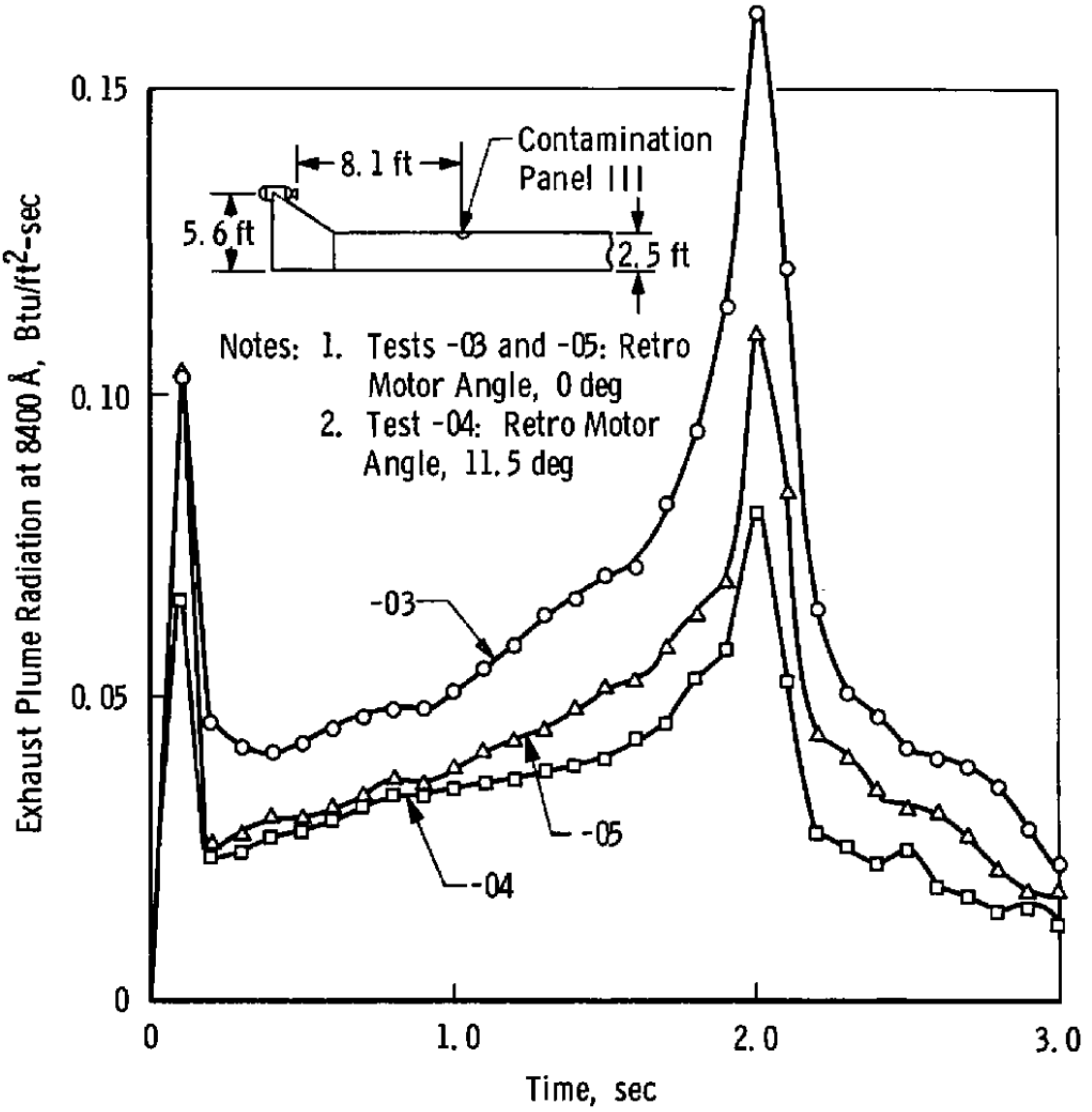

Fig. 27 Contamination Panel III Reflectance of Exhaust Plume Radiance

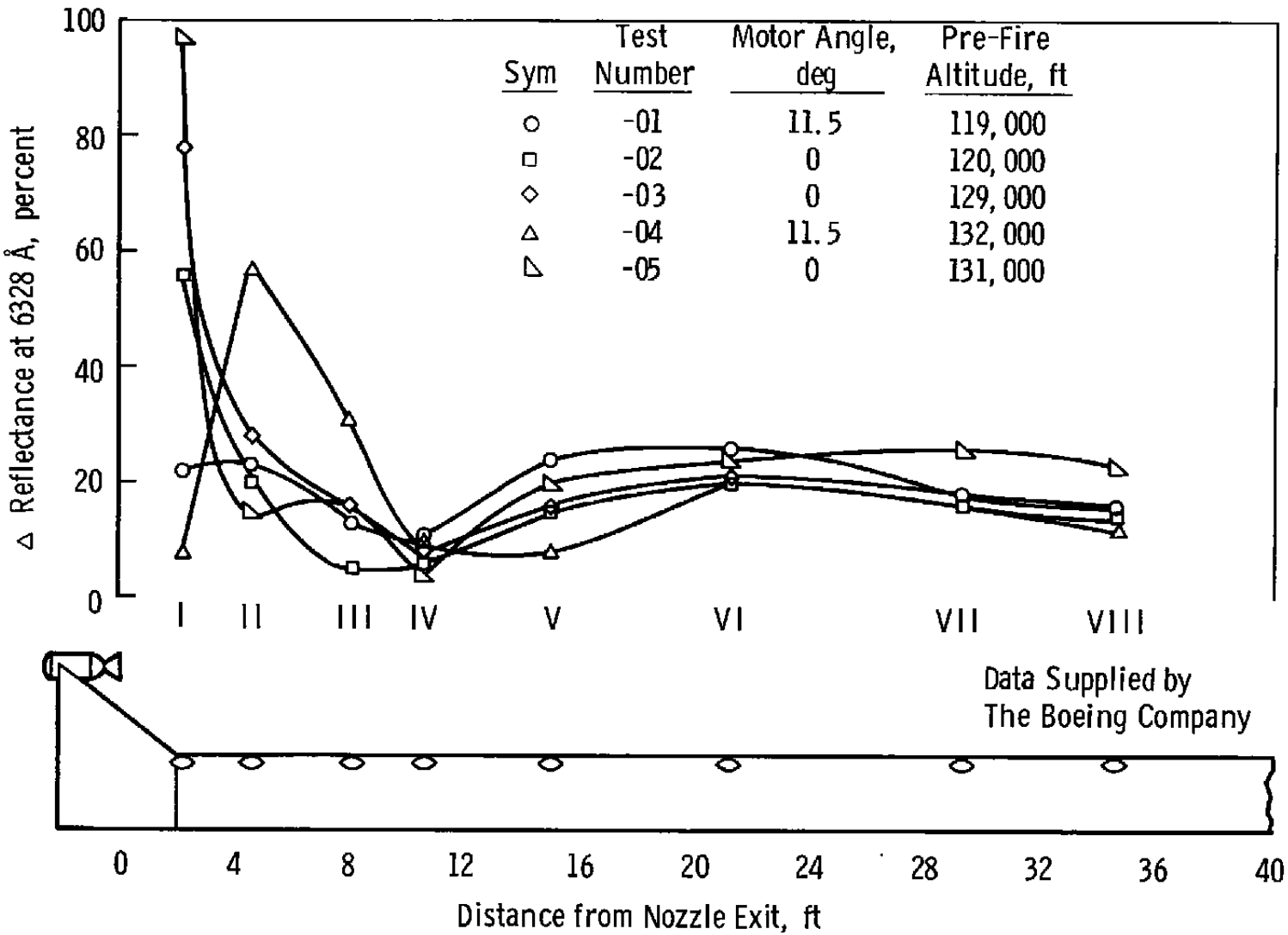

Fig. 28 Total Change in Model Surface Reflectance of a Laser Beam

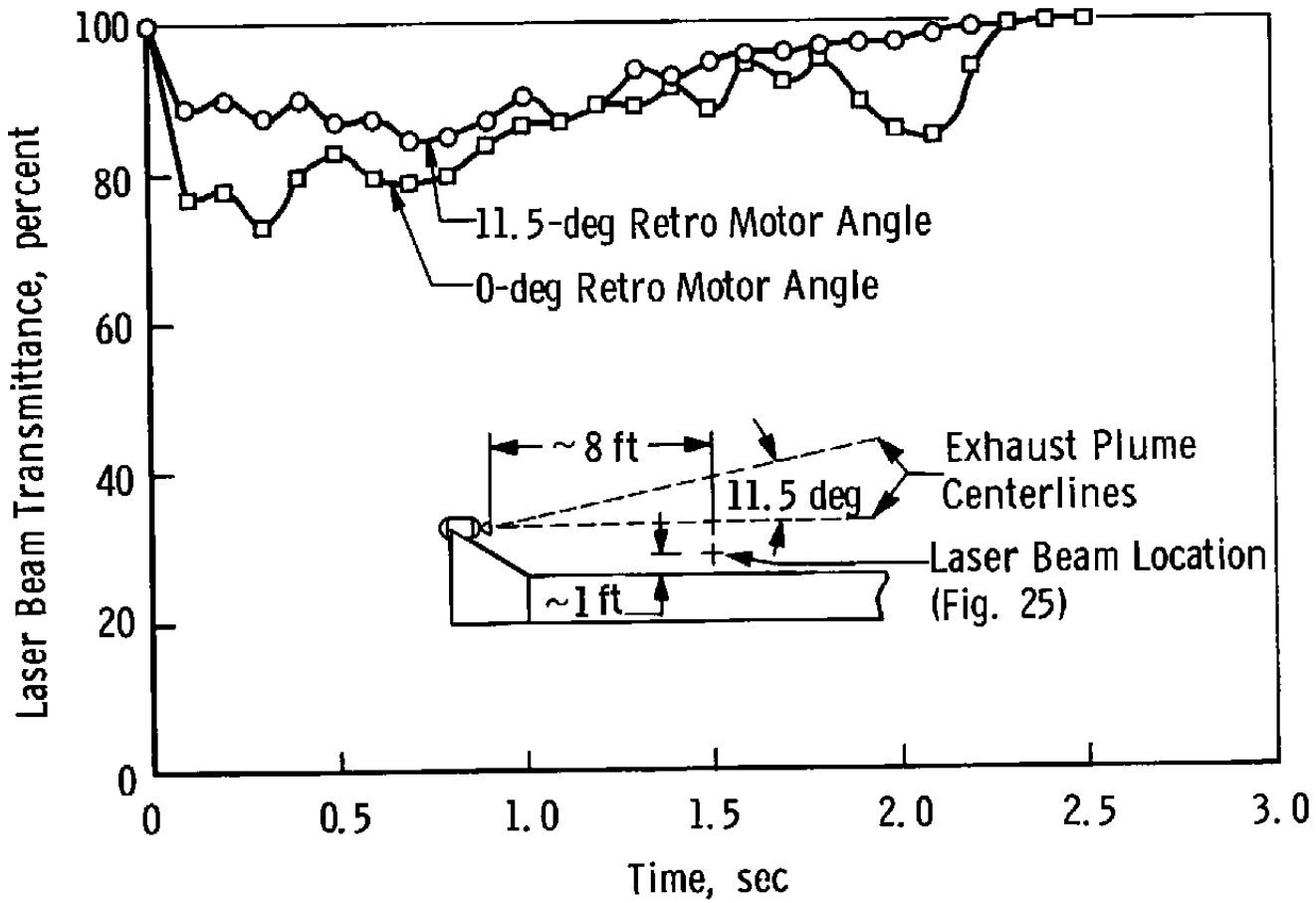

Fig. 29 Laser Beam Transmittance through Exhaust Plumes

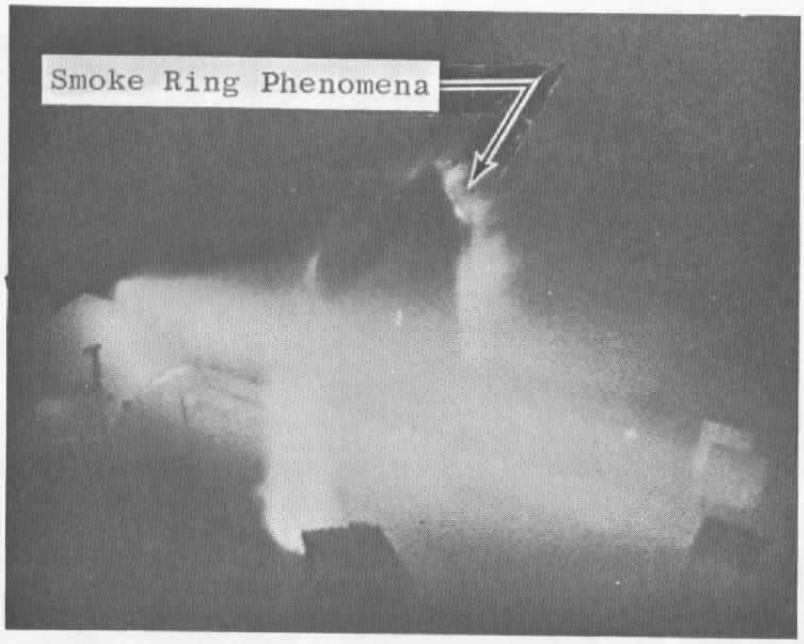

a. t_o + 0.020 sec

b. t_o + 0.028 sec

Fig. 30 Typical Exhaust Plume Characteristics for a 0-deg Angle Retro Motor Firing

c. t_o + 0.032 sec

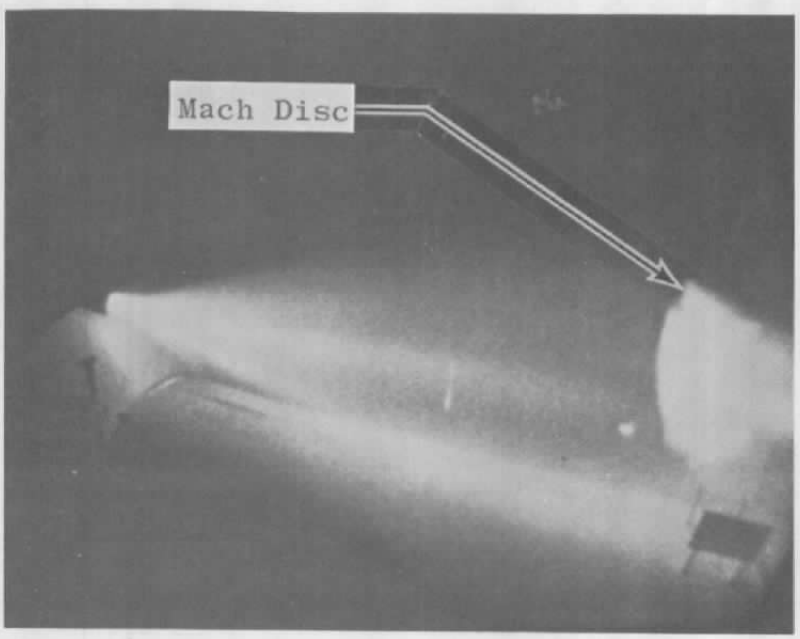

d. t_o + 0.084 sec

Fig. 30 Concluded

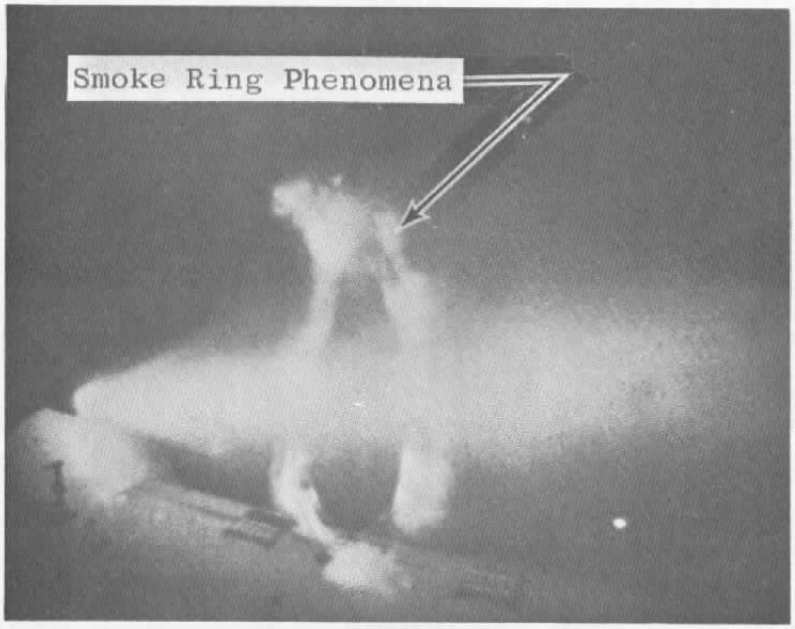

a. t_o + 0.020 sec

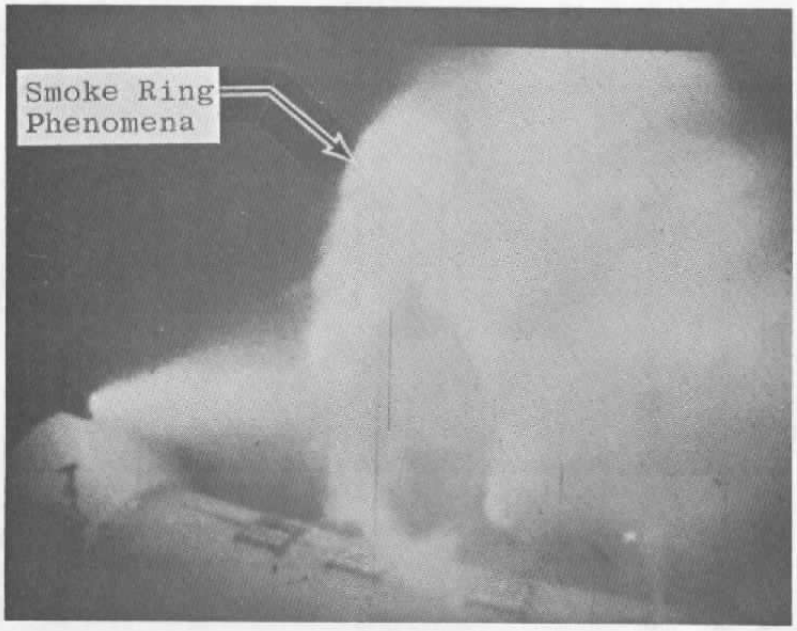

b. t_o + 0.024 sec

Fig. 31 Typical Exhaust Plume Characteristics for an 11.5-deg Angle Retro Motor Firing

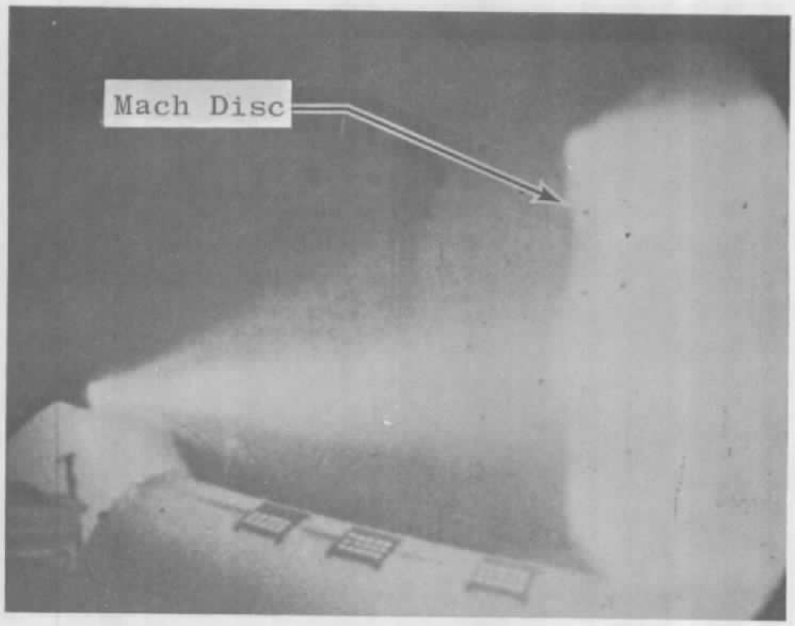

c. t_o + 0.056 sec

d. t_o + 0.544 sec

Fig. 31 Concluded

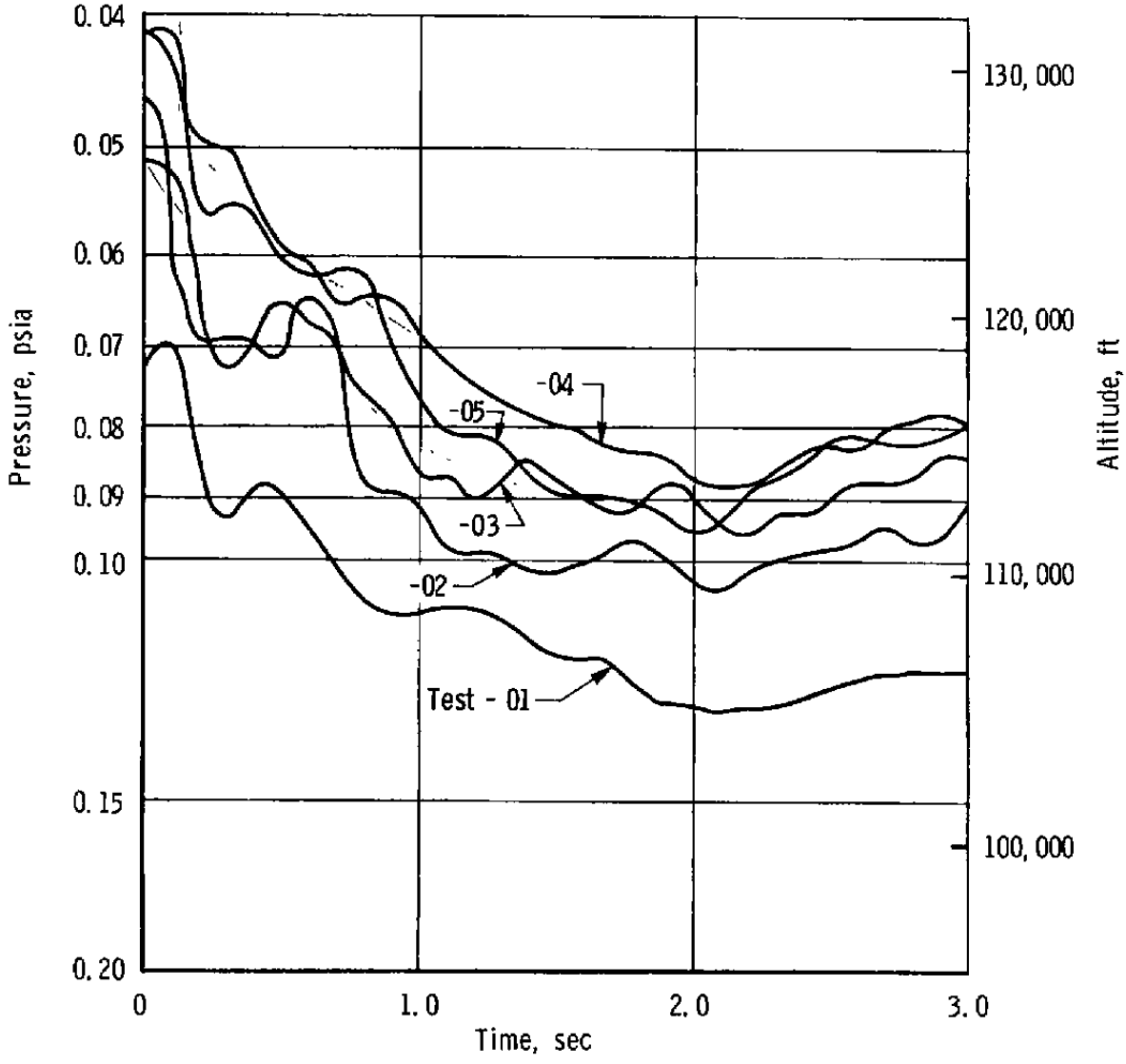

Fig. 32 Motor Ambient Pressure Altitudes

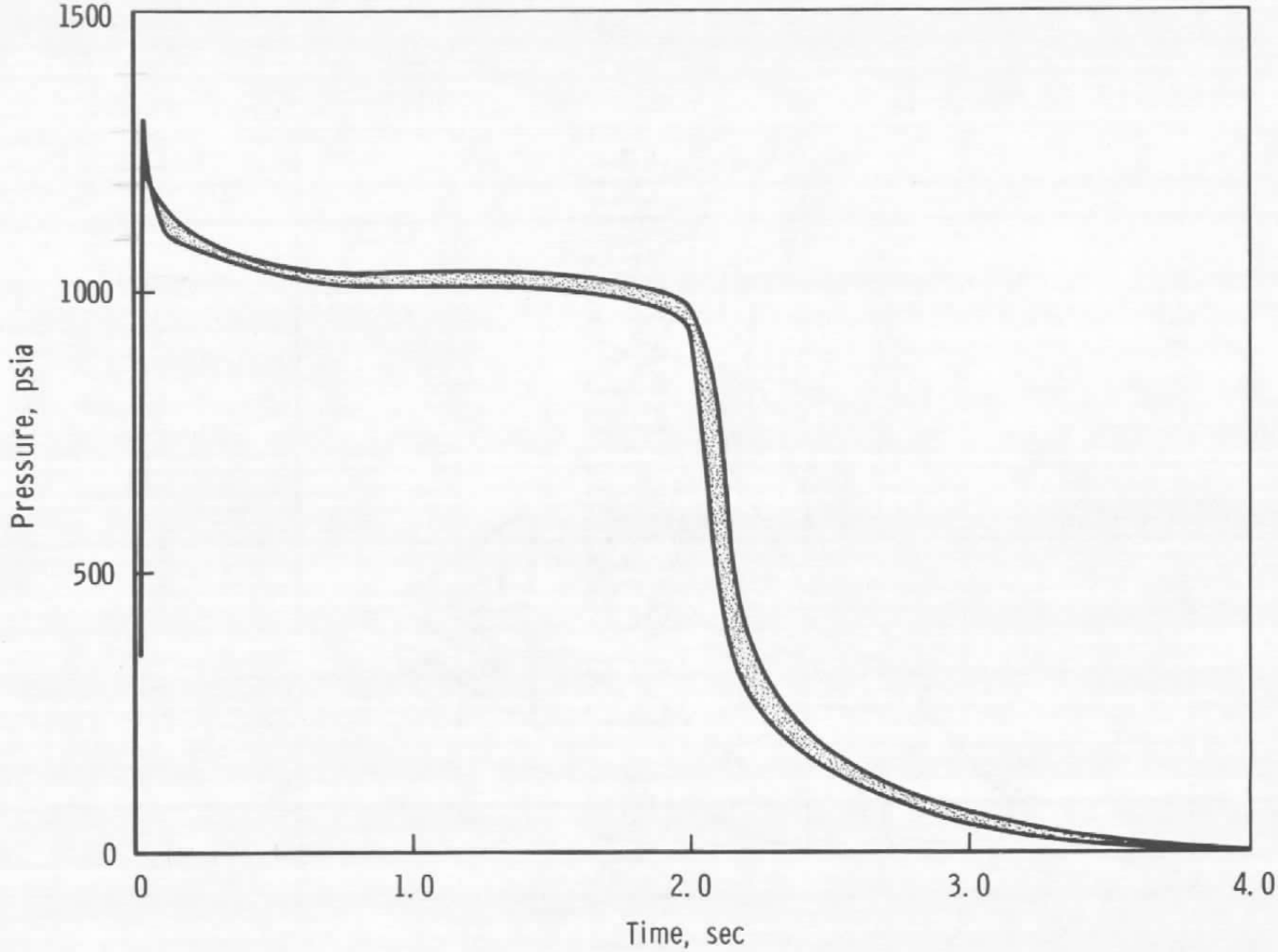

Fig. 33 Motor Chamber Pressure Envelope

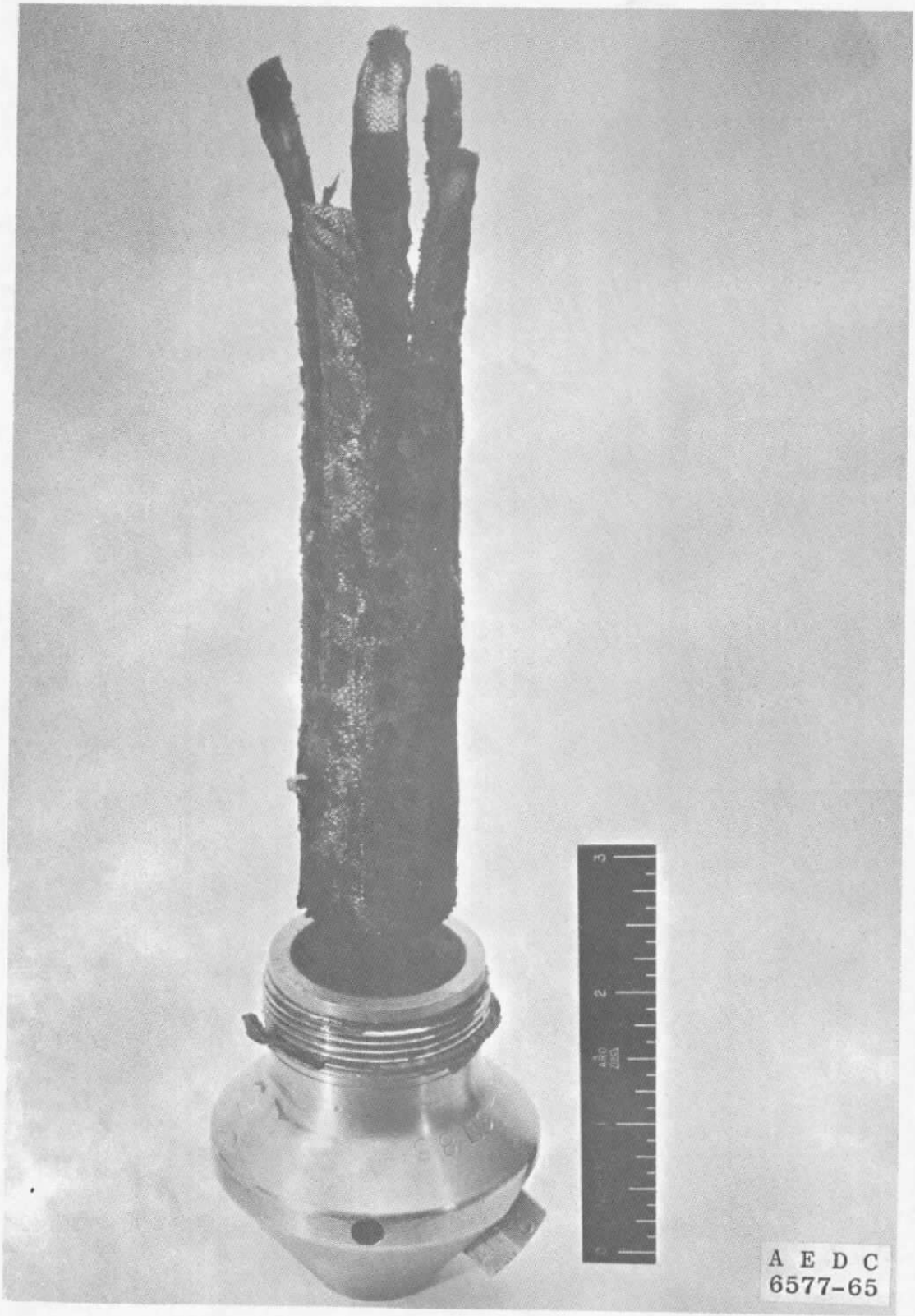

Fig. 34 Typical Spent Igniter

TABLE I
INSTRUMENTATION SUPPLIED BY VARIOUS AGENCIES

Item Number	Type Instrumentation	Furnishing Agency
1	Contamination Panels	
	a. Painted and insulated specimens	NASA/MSFC
	b. Ablative specimens	NASA/MSFC
	c. Disc type	Boeing Company
2	Laser Equipment	Boeing Company
3	Solar Cell Panels and Calibration Rack	NASA/MSFC
4	Heat Flux Transducers	NASA/MSFC
5	Pressure Transducers	NASA/MSFC
6	30, 000-v Transformer and Voltage Divider	Brown Engineering
7	Cinerama Camera	NASA/MSFC

TABLE II
OPTICAL RECORDERS

Firing Number	Camera Type	Designation	Film Speed, frames/sec	Film Type*
-01	Milliken	Camera 1	500	1
	Milliken	Camera 2	500	1
	Cinerama	Camera 3	500	2
	Hulcher	Camera 4	10	3
-02	Milliken	Camera 1	500	1
	Milliken	Camera 2	500	1
	Cinerama	Camera 3	500	2
	Hulcher	Camera 4	10	3
-03	Milliken	Camera 1	500	1
	Milliken	Camera 2	128	4
	Cinerama	Camera 3	64	5
	Hulcher	Camera 4	10	5
	Milliken	Camera 5	32	5
-04	Milliken	Camera 1	500	4
	Millkien	Camera 2	250	4
	Cinerama	Camera 3	200	4
	Hulcher	Camera 4	10	5
	Milliken	Camera 5	---[1]	4
-05	Milliken	Camera 1	128	4
	Milliken	Camera 2	250	4
	Cinerama	Camera 3	150	4
	Hulcher	Camera 4	10	5
	Milliken	Camera 5	128	4

*Film Types

1.	Edgerton XR Extended Range	ASA 400	16 mm
2.	B&W 2475	ASA 1600	16 mm
3.	TRI-X	ASA 400	70 mm
4.	Ektachrome ER 7257	ASA 160	16 mm
5.	Ektachrome ER 7258	ASA 125	16 mm

[1]Failed to operate

TABLE III
SUMMARY OF TEST CONDITIONS AND RESULTS

Firing Number			J4-1548-01	J4-1548-02	J4-1548-03	J4-1548-04	J4-1548-05
Firing Date			11-3-65	11-17-65	11-16-65	11-23-65	11-24-65
Motor Type			TX-143-37	TX-143-37	TX-143-37	TX-143-37	TX-143-37
Motor Serial Number			10104	10105	10112	10114	10113
Igniter Serial Number			1342 1348	1351 1358	1362 1364	1375 1383	1368 1372
Nominal Burn Time, sec			2.0	2.0	2.0	2.0	2.0
Nominal Chamber Pressure, psia			1100	1100	1100	1100	1100
Nominal Thrust, lb_f			5000	5000	5000	5000	5000
Nozzle Exit Area, $in.^2$			18.1	18.1	18.1	18.1	18.1
Nozzle Throat Area, $in.^2$	Pre-Fire Post-Fire		3.58 3.71	3.58 3.67	3.55 3.61	3.56 3.55	3.56 3.64
Motor Weight, lb_f	Pre-Fire Post-Fire		83.4 22.7	83.5 20.7	85.1 24.4	83.7 24.1	83.6 23.9
Motor Ambient Pressure, psia	Pre-Fire Shutdown		0.072 0.132	0.053 0.110	0.046 0.089	0.041 0.089	0.043 0.102
Motor Ambient Pressure Altitude, ft	Pre-Fire Shutdown		119,000 104,500	126,000 108,500	129,000 113,000	132,000 113,000	131,500 110,000
Spray Chamber Temperature, °F	Pre-Fire Maximum		51.2 79.3	52.5 80.1	50.8 80.2	52.3 87.1	52.1 81.1
Motor Cant Angle, Degrees Upward from Model Surface			11.5	0	0	11.5	0
Solar Cel. Panel Mounting Angle, Degrees Relative to Model Surface			0	0	90	*	*
Solar Cells Temperature	Pre-Fire Maximum		51.4 72.7	52.4 124.3	50.9 157.6	*	*
Solar Cells Output Degradation, percent			6.0	26.6	89.7	*	*
Laser Attenuation, percent			‡	‡	‡	12	22
Pressure, psia	Model Surface	P_{ms}-1	0.139	0.280	0.285	0.144	0.292
		P_{ms}-2	0.135	0.234	0.233	0.138	0.240
		P_{ms}-3	0.120	0.180	0.180	0.124	0.192
		P_{ms}-4	0.089	0.125	0.112	0.069	0.130
		P_{ms}-5	0.083	0.113	0.103	0.064	0.105
		P_{ms}-6	0.038	0.039	0.038	0.029	0.036
		P_{ms}-7	0.037	0.036	0.034	0.026	0.029
Total Heat Flux, Btu/ft^2 sec	Model Surface	Q_t-1	4.0	12.8	13.5	9.0	13.8
		Q_t-2	4.6	10.5	10.9	8.5	11.2
		Q_t-3	4.5	7.8	8.0	6.6	8.2
		Q_t-4	4.6	4.8	5.4	5.2	6.1
		Q_t-5	1.2	1.2	1.8	1.2	1.2

‡ Solar Cell Pane, Not Installed
* Invalid Measurement

TABLE IV
TEST SUMMARY OF CONTAMINATION PANELS

Firing Number	Contamination Panel Designation															
	A	B	C	D	E	X	Y	I	II	III	IV	V	VI	VII	VIII	C. P. *
-01	x	x	x	x	x	x	x	x	x	x	x	x	x	x	x	
-02	x	x	x	x	x	x	x	x	x	x	x	x	x	x	x	
-03								x	x	x	x	x	x	x	x	x
-04	x	x	x	x	x	x	x	x	x	x	x	x	x	x	x	
-05						x	x	x	x	x	x	x	x	x	x	x

Data Supplied by The Boeing Company

Remarks

1. Contamination panels A through E contained painted and insulated specimens (Fig. 8a).
2. Contamination panels X and Y contained ablative specimens (Fig. 8b).
3. Contamination panels I through VIII and C. P. were coated with white enamel paint MIL-E-5556 (Fig. 28).

*Charged Panels

TABLE V
MODEL SURFACE REFLECTANCE OF A LASER BEAM

Change in Reflectance, Percent					
Test Number	-01	-02	-03	-04	-05
Panel I	22	56	78	8	97
Panel II	23	20	28	57	15
Panel III	13	5	16	31	16
Panel IV	11	6	8	9	4
Panel V	24	15	16	8	20
Panel VI	26	20	21	20	24
Panel VII	18	16	18	16	26
Panel VIII	16	14	16	12	23

Data supplied by The Boeing Company

Security Classification

DOCUMENT CONTROL DATA - R&D

(Security classification of title, body of abstract and indexing annotation must be entered when the overall report is classified)

1 ORIGINATING ACTIVITY (Corporate author) Arnold Engineering Development Center ARO, Inc., Operating Contractor Arnold Air Force Station, Tennessee	2a REPORT SECURITY CLASSIFICATION UNCLASSIFIED 2b GROUP N/A

3 REPORT TITLE

FULL-SCALE SIMULATED ALTITUDE INVESTIGATION OF THE CENTAUR-PAYLOAD SURFACE AND FUNCTIONAL DEGRADATION RESULTING FROM THE SATURN S-IVB RETRO ROCKET EXHAUST CONTAMINANTS

4 DESCRIPTIVE NOTES (Type of report and inclusive dates)

N/A

5 AUTHOR(S) (Last name, first name, initial)

Muse, W. W., ARO, Inc.

6 REPORT DATE	7a TOTAL NO OF PAGES	7b NO OF REFS
April 1966	78	3

8a CONTRACT OR GRANT NO	9a ORIGINATOR'S REPORT NUMBER(S)
AF40(600)-1200 b PROJECT NO 5991 c System 920E d	AEDC-TR-66-57 9b OTHER REPORT NO(S) (Any other numbers that may be assigned this report) N/A

10 AVAILABILITY/LIMITATION NOTICES Qualified requesters may obtain copies of this report from DDC and transmittal to foreign governments and foreign nationals must have prior approval of NASA, MSFC.

11 SUPPLEMENTARY NOTES	12 SPONSORING MILITARY ACTIVITY
N/A	National Aeronautics and Space Administration (NASA) Marshall Space Flight Center (MSFC) Redstone Arsenal, Alabama

13 ABSTRACT

A series of five tests was conducted in Propulsion Engine Test Cell (J-4) in support of a study to determine the surface contamination of the Centaur vehicle and its payload resulting from the deposition of retro exhaust particles during separation from the spend S-IVB stage. The test article consisted of a full-scale model, 120-deg segment of the S-IVB interstage adapter-Centaur-payload sections of the Saturn 1B-Centaur vehicle. An S-IVB retro motor was mounted in the adapter section at either a 0- or 11.5-deg angle upward from the model surface and was ignited at a pressure altitude of approximately 130,000 ft. The contamination of the model surface was primarily a gray deposit of iron and aluminum oxides. Predominant sizes of the particles deposited on the contamination panels were 1 to 10 μ. However, many particles ranged from 20 to 60 μ, and a few particles were as large as 400 μ. Particle erosion of the paint on the model surface was 12 to 14 μ in depth and occurred in a 4- to 30-ft interval downstream of the nozzle exit. The test results dependent upon retro motor firing angles of 0 and 11.5 deg, respectively, varied as follows: (1) maximum surface heating rate, 14.1 to 9.0 Btu/ft^2-sec; (2) maximum surface pressure, 0.29 to 0.14 psia; (3) degradation of solar cell panel performance, 26.6 to 6.0 percent; (4) laser beam attenuation, 22 to 12 percent; and (5) nominal change in surface reflectance of the model utilizing a laser beam, 27 to 19 percent.

DD FORM 1 JAN 64 1473

Security Classification

14 KEY WORDS	LINK A		LINK B		LINK C	
	ROLE	WT	ROLE	WT	ROLE	WT
Saturn S-IVB						
exhaust						
rocket engine						
surface contamination						
erosion						

INSTRUCTIONS

1. ORIGINATING ACTIVITY: Enter the name and address of the contractor, subcontractor, grantee, Department of Defense activity or other organization *(corporate author)* issuing the report.

2a. REPORT SECURITY CLASSIFICATION: Enter the overall security classification of the report. Indicate whether "Restricted Data" is included. Marking is to be in accordance with appropriate security regulations.

2b. GROUP: Automatic downgrading is specified in DoD Directive 5200.10 and Armed Forces Industrial Manual. Enter the group number. Also, when applicable, show that optional markings have been used for Group 3 and Group 4 as authorized

3. REPORT TITLE: Enter the complete report title in all capital letters. Titles in all cases should be unclassified. If a meaningful title cannot be selected without classification, show title classification in all capitals in parenthesis immediately following the title.

4. DESCRIPTIVE NOTES. If appropriate, enter the type of report, e.g., interim, progress, summary, annual, or final. Give the inclusive dates when a specific reporting period is covered.

5. AUTHOR(S): Enter the name(s) of author(s) as shown on or in the report. Enter last name, first name, middle initial. If military, show rank and branch of service. The name of the principal author is an absolute minimum requirement.

6. REPORT DATE. Enter the date of the report as day, month, year, or month, year. If more than one date appears on the report, use date of publication.

7a. TOTAL NUMBER OF PAGES: The total page count should follow normal pagination procedures, i.e., enter the number of pages containing information.

7b. NUMBER OF REFERENCES: Enter the total number of references cited in the report.

8a. CONTRACT OR GRANT NUMBER: If appropriate, enter the applicable number of the contract or grant under which the report was written.

8b, 8c, & 8d. PROJECT NUMBER: Enter the appropriate military department identification, such as project number, subproject number, system numbers, task number, etc.

9a. ORIGINATOR'S REPORT NUMBER(S): Enter the official report number by which the document will be identified and controlled by the originating activity. This number must be unique to this report.

9b. OTHER REPORT NUMBER(S): If the report has been assigned any other report numbers *(either by the originator or by the sponsor)*, also enter this number(s).

10. AVAILABILITY/LIMITATION NOTICES: Enter any limitations on further dissemination of the report, other than those imposed by security classification, using standard statements such as:

(1) "Qualified requesters may obtain copies of this report from DDC."

(2) "Foreign announcement and dissemination of this report by DDC is not authorized."

(3) "U. S. Government agencies may obtain copies of this report directly from DDC. Other qualified DDC users shall request through

_____."

(4) "U. S. military agencies may obtain copies of this report directly from DDC. Other qualified users shall request through

_____."

(5) "All distribution of this report is controlled. Qualified DDC users shall request through

_____."

If the report has been furnished to the Office of Technical Services, Department of Commerce, for sale to the public, indicate this fact and enter the price, if known.

11. SUPPLEMENTARY NOTES. Use for additional explanatory notes.

12. SPONSORING MILITARY ACTIVITY. Enter the name of the departmental project office or laboratory sponsoring *(paying for)* the research and development. Include address.

13 ABSTRACT. Enter an abstract giving a brief and factual summary of the document indicative of the report, even though it may also appear elsewhere in the body of the technical report. If additional space is required, a continuation sheet shall be attached

It is highly desirable that the abstract of classified reports be unclassified. Each paragraph of the abstract shall end with an indication of the military security classification of the information in the paragraph, represented as *(TS), (S), (C), or (U)*

There is no limitation on the length of the abstract However, the suggested length is from 150 to 225 words.

14. KEY WORDS: Key words are technically meaningful terms or short phrases that characterize a report and may be used as index entries for cataloging the report. Key words must be selected so that no security classification is required. Identifiers, such as equipment model designation, trade name, military project code name, geographic location, may be used as key words but will be followed by an indication of technical context The assignment of links, rules, and weights is optional.

DEPARTMENT OF THE AIR FORCE
HEADQUARTERS ARNOLD ENGINEERING DEVELOPMENT CENTER (AFSC)
ARNOLD AIR FORCE STATION, TENNESSEE 37389

REPLY TO ATTN OF: AETI

13 June 66

SUBJECT: Distribution Statement on AEDC TR-66-57

TO: ARO, Inc.
Attn: Joe Ashley, Jr., ESF (TIB)
Arnold AF Stn, Tenn

1. It is requested that the distribution statement as contained in TR-66-57 be amended to read as follows:

> This document is subject to special export controls and each transmittal to foreign governments or foreign nationals may be made only with prior approval of NASA, Marshall Space Flight Center and AEDC.

2. Please notify all recipients of this report of this change.

R. L. Kindley

for LEONARD T. GLASER, COL, USAF
Assistant DCS/Test